J. Mol. Biol. (1993) **231**, 82–102

Exploring the Limits of Precision and Accuracy of Protein Structures Determined by Nuclear Magnetic Resonance Spectroscopy

G. Marius Clore, Mark A. Robien and Angela M. Gronenborn

Laboratory of Chemical Physics, Building 5
National Institute of Diabetes and Digestive and Kidney Diseases
National Institutes of Health, Bethesda, MD 20892, U.S.A.

(Received 7 September 1992; accepted 12 January 1993)

The effects of the number, precision and accuracy of interproton distance restraints, of direct refinement against nuclear Overhauser enhancement (NOE) intensities and of the description of the non-bonded contacts on the precision and accuracy of a nuclear magnetic resonance (NMR) protein structure determination have been investigated. The model system employed is the 56 residue immunoglobulin G binding domain of streptococcal protein G. This choice was based on the availability of a very high resolution NMR structure (atomic root-mean-square distribution of the ensemble of 60 calculated structures about the mean co-ordinate positions of 0·25 Å for the backbone atoms, 0·65 Å for all atoms and 0·39 Å for all atoms excluding disordered surface side-chains). The experimental NMR data set for this structure determination comprised a total of 1058 experimental restraints of which 854 were approximate interproton distance restraints corresponding to all the structurally useful NOEs observable for this protein. The calculations presented in this paper reveal the following. (1) The number of interproton distance restraints constitutes the single most important determinant of both precision and accuracy. The ensemble precision and accuracy improves significantly as the number of interproton distance restraints is increased to an average of ~15 per residue, of which ~60% involve unique proton pairs; subsequent additions of interproton distance restraints, however, lead to less dramatic improvements as information redundancy sets in. (2) The ratio of ensemble precision to ensemble accuracy (which ranges from 0·5 to 0·7 for the backbone atoms) is approximately independent both of the number, precision and accuracy of the interproton distance restraints, and of whether the structures are refined against interproton distance restraints or directly against NOE intensities. (3) In an ensemble of structures generated from a large number of loose approximate interproton distance restraints (an average of ~15 restraints per residue with ~60% involving unique proton pairs), the interproton distance vectors corresponding to the restraints are very well defined with ~80% of vectors between unique proton pairs having a standard deviation of ≤0·1 Å. (4) The accuracy of the mean co-ordinates of an ensemble of structures is significantly higher than the average accuracy of the individual structures comprising the ensemble. For an average ensemble precision of ≥0·6 Å, the dependence of the accuracy of the mean co-ordinates on ensemble precision is approximately linear. As the ensemble precision, however, increases beyond ~0·6 Å, the dependence is asymptotic and the accuracy of the mean co-ordinates reaches a limiting value of ~0·1 Å. (5) There is no significant difference in the results obtained with precise interproton distance restraints *versus* those with loose approximate interproton distance restraints. (6) The ensemble precision of a structure determination can potentially be improved by the use of either accurate (as opposed to simply precise) interproton distance restraints or by direct refinement against NOE intensities; the former, however, cannot be obtained experimentally, while the latter can potentially introduce systematic errors unless effects of internal motions are taken into account appropriately. This increase in precision, however, is not necessarily reflected by a corresponding increase in the accuracy of the mean co-ordinates. Hence, in practice, direct refinement against NOE intensities is unlikely to have a significant impact in terms of attainable accuracy over the use of the much simpler and computationally much more efficient loose approximate interproton distance restraints for all but a very few exceptional cases. (7) Neglecting the effects of the non-bonded contacts, the maximum ensemble accuracy that can be achieved in practice is ~0·25 to

0022–2836/93/090082–21 $08.00/0

0·30 Å for the backbone atoms. (8) The description of the non-bonded contacts can have a profound effect on both the precision and accuracy of the resulting structures, and when these effects are taken into account, the likely practical limit on the attainable ensemble accuracy is 0·4 to 0·6 Å for the backbone atoms, 0·8 to 1·1 Å for all atoms and 0·5 to 0·8 Å for all ordered atoms, with the corresponding accuracy of the mean co-ordinates being 0·1 to 0·2 Å better.

Keywords: protein structure; NMR; accuracy; precision; NOE

1. Introduction

Over the past few years significant advances have been made in increasing both the precision and molecular weight range of protein structures determined by nuclear magnetic resonance (NMR†) spectroscopy (for reviews, see Clore & Gronenborn, 1991*a*,*b*). For example, it has been shown in the case of interleukin-1β, a protein of 153 residues, that the positional errors in the atomic co-ordinates of the high resolution NMR structure (Clore *et al.*, 1991), determined on the basis of 3146 approximate experimental restraints, are comparable to those of three independent X-ray structures solved at 2 Å (1 Å = 0·1 nm) resolution (Clore & Gronenborn, 1991*c*). This high degree of precision was achieved by making use of three- and four-dimensional heteronuclear NMR spectroscopy to obtain the maximum number of structurally useful interproton distance restraints from NOE data, and systematic conformational grid search procedures to obtain stereospecific assignments and ϕ, ψ and χ_1 torsion angle restraints from NOE and coupling constant data. All these experimental restraints were specified as loose ranges. Thus, the interproton distance restraints were classified into three ranges, 1·8 to 2·7 Å, 1·8 to 3·3 Å and 1·8 to 5·0 Å, corresponding to strong, medium and weak NOEs; likewise, the minimum ranges employed for the ϕ, ψ and χ_1 restraints were $\pm 30°$, $\pm 50°$ and $\pm 20°$, respectively. In an effort to further increase the precision of NMR structures it has been suggested that either more accurate interproton distance restraints derived from an interactive relaxation matrix analysis of the NOE intensities (Borgias & James, 1988, 1990; Boelens *et al.*, 1988, 1989; Post *et al.*, 1990; Borgias *et al.*, 1990; Thomas *et al.*, 1991) or direct refinement against the NOE intensities (Yip & Case, 1989; Nilges *et al.*, 1991) should be employed.

In the present paper, we set out to analyze the practical limits of precision and accuracy that are attainable in NMR protein structure determinations and to delineate the factors that have the greatest bearing on them. To this end, we have carried out a series of model calculations on the IgG binding domain of streptococcal protein G, a protein of 56 residues, for which a very high resolution NMR structure is available (Gronenborn *et al.*, 1991). The structure published originally was based on 1058 experimental restraints comprising 854 NOE derived approximate interproton distance restraints, 60 distance restraints for 30 backbone hydrogen bonds and 144 torsion angle restraints. The atomic r.m.s. distribution of the ensemble of 60 simulated annealing structures about the mean co-ordinate positions was 0·25 Å for the backbone atoms, 0·65 Å for all atoms, and 0·39 Å for all atoms excluding those of disordered surface side-chains. To our knowledge, this structure represents the most precise experimental NMR structure determination published to date using conservative approximate experimental restraints. Further, the NOE restraints are complete in so far that every single cross-peak in the NOESY spectra was assigned. Hence, the collection of 854 NOE restraints used in the structure calculations comprises all the structurally useful NOEs that are observable for this protein (i.e. they do not include, for example, intra-residue interproton distance restraints between protons whose separation is fixed by covalent geometry or between non-stereospecifically assigned protons separated by three bonds). Thus, this experimental data set provides an ideal system for investigating the effects of the (1) number, (2) precision and (3) accuracy of the interproton distance restraints, of (4) direct refinement against model NOE intensities, and of (5) alterations in the description of the non-bonded contacts on the precision and accuracy of the resulting ensemble of calculated structures.

2. Calculational Strategy

(a) *The source data*

The data for the present investigation comprises the 60 simulated annealing structures (PDB accession code 2GB1) and the restrained minimized mean structure, $(SA)_{r854}$ (PDB accession code 1GB1) of the IgG binding domain of protein G published by Gronenborn *et al.* (1991), together with the set of 1058 experimental restraints (PDB accession code R1GB1MR) used to calculate these structures. The latter comprise 854 structurally useful, approximate NOE interproton distance restraints which are subdivided into 146 sequential ($|i-j|=1$), 108 short range ($1<|i-j|\leq 5$) and 291 long-range ($|i-j|>5$) interresidue restraints, and 309 intraresidue restraints. In addition, there were 60 distance restraints ($r_{NH\cdot O}\leq 2{\cdot}3$ Å and $r_{N\cdot O}=2{\cdot}5$ to 3·3 Å) for

† Abbreviations used: NMR, nuclear magnetic resonance; NOE, nuclear Overhauser effect; NOESY, nuclear Overhauser enhancement spectroscopy; r.m.s., root-mean-square; SA, simulated annealing; Ig, immunoglobulin; PDB, Protein Data Bank; 3D, 4D, 3-dimensional, 4-dimensional, respectively.

30 hydrogen bonds involving slowly exchanging backbone amide protons, and 144 torsion angle restraints (54 ϕ, 51ψ and 39 χ_1 angles with minimum ranges of $\pm 30°$, $\pm 50°$ and $\pm 20°$, respectively, derived from the experimental NOE and three-bond coupling constant data by means of a systematic conformational grid search of ϕ, ψ, χ_1 space). The 854 NOE interproton distance restraints in the original publication were classified into three ranges, 1·8 to 2·7 Å, 1·8 to 3·3 Å (1·8 to 3·5 Å for NOEs involving NH protons) and 1·8 to 5·0 Å, corresponding to strong, medium and weak NOEs, respectively, with appropriate corrections for center averaging added to the upper bounds of distance restraints involving methyl protons and non-stereospecifically assigned protons. The NOE target function was represented by a square-well quadratic potential, F_{NOE}, with center averaging given by Clore *et al.* (1986*a*):

$$F_{NOE} = \sum \begin{cases} k_{NOE}(R_{ij} - r^u_{ij})^2, & \text{if } R_{ij} > r^u_{ij} \\ 0, & \text{if } r^l_{ij} \le R_{ij} \le r^u_{ij} \\ k_{NOE}(R_{ij} - r^l_{ij})^2, & \text{if } R_{ij} < r^l_{ij}, \end{cases} \quad (1)$$

where R_{ij} is the calculated distance between protons i and j, r^u_{ij} and r^l_{ij} are the values of the upper and lower limits of the target distances, respectively, and k_{NOE} is the NOE force constant. The NOE data set included stereospecific assignments for 24 of the 30 β-methylene protons, for the α-methylene protons of all four Gly residues, and for the methyl groups of three of the four Val residues and two of the three Leu residues. In addition, although the ^{1}H chemical shifts of the methyl groups of Val21 and Leu7 and of the aromatic ring protons on either side of the Tyr and Phe rings were degenerate, many of the NOEs involving these protons could be stereospecifically assigned on the basis of the initial structures. Finally, it should be noted that the χ_1 side-chain torsion angles for the six residues whose β-methylene protons were not stereoassigned are conformationally disordered on the basis of $^3J_{\alpha\beta}$ coupling constants of 6 to 7 Hz.

(b) *Generation of data sets with accurate or precise NOE distance restraints*

To simulate the effect of highly accurate or precise NOE distance restraints, we used the 60 simulated annealing (SA) structures of Gronenborn *et al.* (1991) (PDB accession code 2GB1) to calculate the mean and standard deviation (σ) of the interproton distances corresponding to the 854 structurally useful, experimentally assigned NOEs. We then replaced the conservative approximate NOE distance restraints with restraints based on the calculated means and moments of the corresponding interproton distances in the 60 SA structures. For NOE restraints involving two uniquely identified protons (e.g. methine, stereoassigned methylene or backbone amide protons), the calculation of the mean and standard deviation of the interproton distance is straightforward. For other protons (e.g. methyl protons, non-stereospecifically assigned methylene and aromatic ring protons), it is necessary to correct the means and standard deviations appropriately. This was accomplished by using the $\langle r^{-6} \rangle^{-1/6}$ mean of all the interproton distances corresponding to the protons specified in the NOE restraints file. The resulting standard deviation thus contained a contribution from the variance of the means. The means and standard deviations of the interproton distances were calculated to the nearest 0·001 Å, and the NOE restraints files recoded using the resulting mean interproton distance as the target distance and twice the standard deviation (2σ) as the characteristic half-width for the interproton distance potential in the simulated annealing protocol.

The large majority of these interproton distances are, in fact, very well defined in the 60 SA structures, as evidenced by very small standard deviations in their values (see Fig. 1 and Table 1). Of the 543 distances between unique proton pairs (even including those with values between 5 and 6 Å), 78% and 94% had a standard deviation of less than 0·1 Å and 0·2 Å, respectively (Fig. 1A and Table 1). Further, 23 of the 103 long-range (5 to 6 Å) distances had a standard deviation of less than 0·1 Å. Not surprisingly, the values of the standard deviations are larger for the 311 distances involving methyl groups or non-stereospecifically assigned protons (Fig. 1B), with the largest deviations being restricted to distances involving disordered surface side-chains. However, even for these distances, 87% had a standard deviation of less than 1·0 Å (Table 1). Thus, the standard deviations of the interproton distance vectors for the 60 SA structures that correspond to the approximate interproton

Table 1

Distribution of standard deviations of the interproton distance vectors observed in the ensemble of 60 SA structures of the IgG binding domain of protein G (PDB accession code 2GB1) corresponding to the 854 approximate interproton distance restraints (PDB accession code R1GB1MR) used in their calculation

	Number of distances (percentage of total)	
Standard (Å)	Distances between unique proton pairs (total no. = 543)	Distances involving methyl protons or non-stereospecifically assigned protons (total no. = 311)
<0·01	62 (11·4%)	0 (0·0%)
0·01–0·10	360 (66·3%)	3 (1·0%)
0·10–0·20	87 (16·0%)	5 (1·6%)
0·20–0·50	28 (5·2%)	48 (15·4%)
0·50–1·00	6 (1·1%)	214 (68·8%)
1·00–2·00	0 (0·0%)	34 (10·9%)
2·00–3·00	0 (0·0%)	7 (2·3%)

The 854 interproton distance restraints comprise 146 sequential ($|i-j|=1$), 108 short-range ($1<|i-j|\le 5$) and 291 long-range ($|i-j|>5$) interresidue restraints and 309 intraresidue restraints.

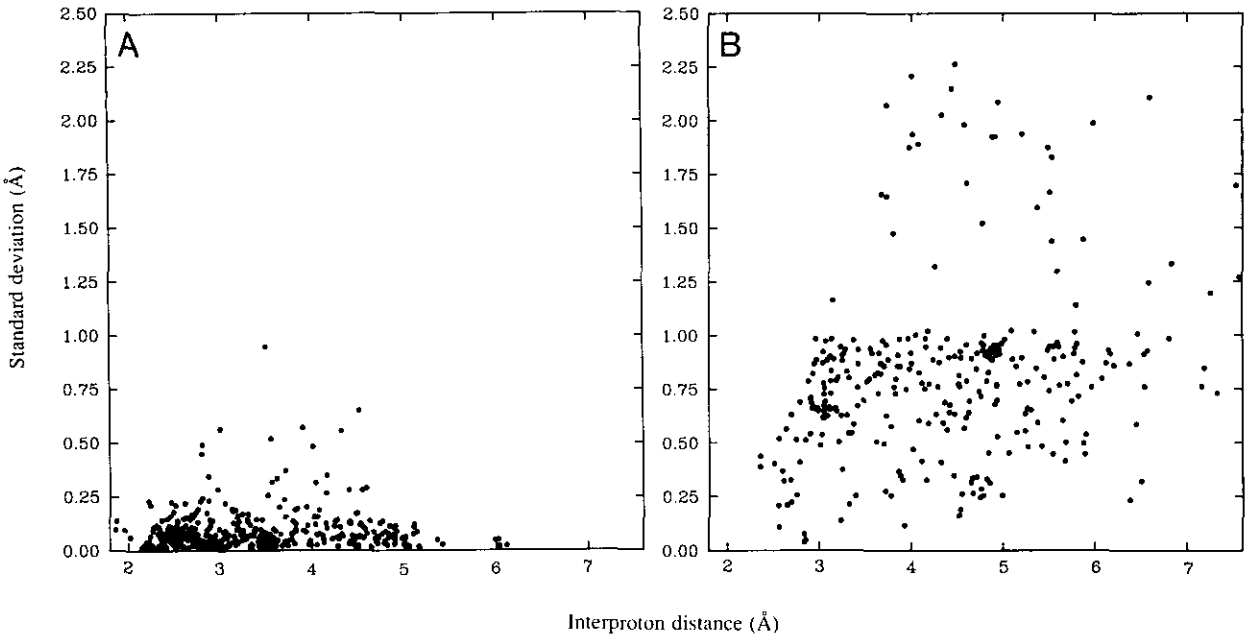

Figure 1. Variation of standard deviation *versus* distance for the interproton distance vectors observed in the ensemble of 60 SA structures of the IgG binding domain of protein G (PDB accession code 2GB1) corresponding to the 854 approximate interproton distance restraints (PDB accession code R1GB1MR) used in their calculation. A, The data for the 543 distances between unique proton pairs; B, the data for the 311 distances involving methyl protons or non-stereo-assigned protons.

distance restraints used in the calculation of these structures are, in fact, significantly smaller than the likely errors arising from attempts to obtain accurate or precise interproton distance restraints experimentally through such procedures as inter-active relaxation matrix analysis of the NOE intensities (Borgias & James, 1990; Borgias *et al.*, 1990; Post *et al.*, 1990).

This result may at first seem a little surprising, but goes hand in hand with the high precision of the atomic co-ordinates of the structures calculated with the approximate interproton distance restraints. This stems from the fact that although the distance restraints are approximate, taken as a whole they are conformationally restrictive owing to two factors acting in concert: (1) many of the vectors corresponding to the interproton distance restraints are highly correlated, and (2) short distance restraints (<5 Å) between residues far apart in the sequence severely limit the conformational space accessible to the polypeptide chain (Clore & Gronenborn, 1989*a*).

To simulate the effect of "accurate" interproton distance restraints we employed a harmonic quadratic NOE potential with $\langle r^{-6}\rangle^{-1/6}$ averaging given by Clore *et al.* (1985):

$$F_{\mathrm{NOE}} = \sum \frac{S_{\mathrm{NOE}} k_{\mathrm{B}} T}{2c_{ij}^2} (R_{ij} - d_{ij})^2, \qquad (2)$$

where S_{NOE} is a scale factor, k_{B} the Boltzmann constant, T the temperature in the simulated annealing schedule, R_{ij} the calculated interproton distance, d_{ij} the "equilibrium" target distance (set to the mean interproton distance found in the 60 SA structures calculated using all 854 approximate interproton distance restraints), and c_{ij} the characteristic distance for the harmonic potential set to 2σ of the interproton distances in the 60 SA structures. Thus, $F_{\mathrm{NOE}} = 0$ only when the calculated distance R is equal to the target distance d.

To assess the effect of precise distance restraints we employed a restrictive square-well quadratic potential (Clore *et al.*, 1986*a*) which assigns no contribution to F_{NOE} whenever the interproton distance is within two standard deviations (σ) of the mean value:

$$F_{\mathrm{NOE}} = \sum \begin{cases} 0 & \text{if } |R_{ij} - d_{ij}| \le 2\sigma_{ij} \\ k_{\mathrm{NOE}}(|R_{ij} - d_{ij}| - 2\sigma_{ij})^2, & \text{if } |R_{ij} - d_{ij}| > 2\sigma_{ij}. \end{cases} \qquad (3)$$

(c) *Generation of data sets with different numbers of NOE restraints*

To evaluate the effect of the number of NOE restraints on the precision and accuracy of the ensemble of resulting simulated annealing structures, ten randomly shuffled sets of all 854 NOE restraints were generated; 64% of the 854 restraints are between unique proton pairs, while the remaining 37% involve either methyl and/or non-stereospecifically assigned protons. Because of random sampling, this distribution, as well as that between intra- and interresidue restraints, and between sequential ($|i-j| = 1$), short-range ($1 < |i-j| \le 5$) and long-range ($|i-j| > 5$) inter-residue restraints, is approximately preserved in all the smaller subsets of restraints. Subsets of four different sizes comprising 76, 107, 153 and 300

restraints, corresponding to an average of 1·36, 1·91, 2·73 and 5·36 restraints per residue, respectively, were then collected by selecting the appropriate number of restraints from the shuffled restraints files, and used in a series of simulated annealing calculations with the three different interproton distance potentials (i.e. accurate harmonic, precise square-well and approximate square-well). Thus, a total of 40 different subsets of NOE interproton distance restraints were used, in addition to the complete set comprising all 854 interproton distance restraints. The number of structures calculated for the different types of interproton distance restraints were as follows. For both the accurate and precise sets of restraints, a structure corresponding to each subset of restraints was calculated, in addition to ten structures calculated for the complete set of restraints, making a total of 50 structures with ten structures for each size category. (Note that in the ensemble of structures calculated with 76 and 107 precise interproton distance restraints, one calculation in each case failed to converge and was therefore excluded from subsequent analysis.) For the approximate set of restraints, two structures corresponding to each subset of restraints were calculated, yielding 20 structures for each size category ranging from 76 to 300 restraints, in addition to the 60 original structures for the complete set of restraints, making a total of 140 structures.

(d) *Calculation of structures with interproton distance restraints*

Ensemble of structures with the different number and types of interproton distance restraints were calculated using the simulated annealing protocol of Nilges *et al.* (1988) with the program XPLOR (Brünger *et al.*, 1986, 1987; Brünger, 1992*a*). In addition to a potential term for the NOE interproton distance restraints, this protocol employs the following terms. Quadratic harmonic potential terms (with force constants of 500 kcal·mol^{-1}·Å^{-2} and 500 kcal·mol^{-1}·rad^{-2} for bond and angular terms, respectively; 1 cal = 4·184 J) are used to maintain the covalent geometry very close to ideality. The non-bonded contacts are described by a quartic van der Waals repulsion term, F_{repel}, given by:

$$F_{repel} = \begin{cases} 0, & \text{if } r \geq s_{vdw}(r_{vdw,i}+r_{vdw,j}) \\ k_{vdw}\{[s_{vdw}(r_{vdw,i}+r_{vdw,j})]^2 - r^2\}^2, & \text{if } r < s_{vdw}(r_{vdw,i}+r_{vdw,j}), \end{cases} \quad (4)$$

where k_{vdw} is a variable force constant, r is the distance between two atoms, $r_{vdw,i}$ and $r_{vdw,j}$ are the standard values of the van der Waals radii of atoms i and j, respectively, as represented by the Lennard–Jones potential used in the CHARMM PARAM19 and PARAM20 empirical energy function (Brooks *et al.*, 1983; Reiher, 1985) (a list of the hard sphere van der Waals radii is provided in Table 2), and s_{vdw} is a van der Waals radius scale factor to account for the fact that interatomic separations slightly smaller than the sum of the hard sphere radii can easily occur owing to the attractive component of the van der Waals interaction. In computing equation (4), 1–2 and 1–3 interactions are excluded from the non-bonded list. A square-well quadratic potential is used for the experimental torsion (ϕ, ψ and χ_1) angle restraints and is given by Clore *et al.* (1986*a*):

$$F_{tor} = \sum \begin{cases} k_{tor}(\Delta_i - \Delta_i^u)^2, & \text{if } \Delta_i > \Delta_i^u \\ 0, & \text{if } \Delta_i^l \leq \Delta_i \leq \Delta_i^u \\ k_{tor}(\Delta_i - \Delta_i^l)^2, & \text{if } \Delta_i < \Delta_i^l, \end{cases} \quad (5)$$

where Δ_i^u and Δ_i^l are the upper and lower limits of the target range of a particular torsion angle, respectively, Δ_i is its calculated value, and k_{tor} a force constant. Finally, a square-well quadratic potential (given by eqn (1)) is employed for the hydrogen bonding distance restraints derived experimentally on the basis of the NOE and NH exchange data.

To simplify the analysis, all the simulated annealing calculations included the 60 hydrogen bonding distance restraints and the 144 torsion angle restraints employed in the original structure determination of Gronenborn *et al.* (1991). The protocol employed proceeded in four phases: (1) 200 cycles of Powell minimization with $k_{NOE} = 0$ kcal·mol^{-1}·Å^{-2} (eqns (1) or (3)) or $S_{NOE} = 0$ (eqn (2)), $k_{tor} = 0$ kcal·mol^{-1}·rad^{-2}, $s_{vdw} = 1·0$ and $k_{vdw} =$ 0·001 kcal·mol^{-1}·Å^{-4}; (2) 3·75 ps of dynamics at 1000 K (with a time step of 1 fs and coupling to a heat bath) during which time k_{NOE}, S_{NOE} (if applicable) and k_{tor} were increased from 0·5 to 30 kcal·mol^{-1}·Å^{-2}, 0·5 to 30, and 0·5 to 200 kcal·mol^{-1}·rad^{-2}, respectively, by doubling their values every 75 fs, and k_{vdw} was increased from 0·001 to 0·25 kcal·mol^{-1}·Å^{-4} by multiplying its value by 1·125 every 75 fs with the van der Waals radius scale factor s_{vdw} maintained at a constant value of 1·0; 1·5 ps of dynamics during which time the

Table 2

Values of hard sphere van der Waals radii (r_{vdw}) used in the present work

	r_{vdw} (Å)	r_{vdw}(eff) (Å) for $s_{vdw} = 0·8$†	r_{vdw}(Dis) (Å)‡
H polar	0·80	0·64	0·95
H non-polar	1·46	1·17	1·00
N	1·55	1·24	1·30
C	1·80	1·44	1·40 (1·35 for aromatic C)
O	1·48	1·19	1·20
S	1·90	1·52	1·60

The hard sphere radii are those used in the CHARMM PARAM19/PARAM20 energy parameters (Brooks *et al.*, 1983; Reiher, 1985).

† The effective hard sphere van der Waals radius r_{vdw}(eff) is given by $s_{vdw} \cdot r_{vdw}$ (cf. eqn (4)).

‡ r_{vdw}(Dis) are the hard sphere van der Waals radii employed by the programs DISMAN (Braun & Go, 1985) and DIANA (Güntert *et al.*, 1991).

system was cooled to 300 K in steps of 25 deg.K every 50 fs, with the van der Waals repulsion terms k_{vdw} and s_{vdw} set to 4 kcal·mol^{-1}·Å^{-4} and 0·8, respectively, and the force constants for the NOE and torsion angle terms set to the same values reached at the end of phase (2); and finally 500 steps of Powell minimization with the same force constants used in phase (3).

To facilitate the calculations and ensure high convergence, the starting structures for the simulated annealing were chosen from the ensemble of the original set of 60 calculated structures published by Gronenborn *et al.* (1991) and different random number seeds were used in each case for the assignment of initial velocities to a Boltzman distribution. While this choice of initial structures may at first appear to limit sampling, extensive experience with the present protocol indicates that the use of high temperature and an initially very low value for the van der Waals repulsion force constant k_{NOE} during phase (2) of the protocol (which, for example, enables interpenetration of peptide chains) permits very efficient sampling of the conformational space consistent with the experimental restraints (Nilges *et al.*, 1988; Clore & Gronenborn, 1989*a*). To verify this assertion, some trial simulated annealing calculations with the subsets of 76, 107, 153 and 300 approximate restraints were carried out using ten different substructures (comprising about one-third of the atoms) obtained by projection from n-dimensional distance space into cartesian co-ordinate space with one of the sets of 76 approximate interproton distance restraints, by means of the distance geometry module of XPLOR (Kuszewski *et al.*, 1992). The resulting accuracy and precision of the trial structures obtained in this manner was not different, within experimental error, from those obtained using starting structures from the original ensemble of 60 simulated annealing structures.

(e) *Assessment of the effect of the van der Waals radius scale factor*

To assess the effect of the van der Waals radius scale factor, s_{vdw}, on the precision and accuracy of the resulting structures, a series of simulated annealing calculations were carried out with the full set of 854 approximate interproton distance restraints, together with the other experimental restraints, using various values of s_{vdw} in phases (3) and (4) of the simulated annealing protocol. All other aspects of the simulated annealing protocol were as described above. Twenty structures were calculated for each of four different values of s_{vdw} (0·7, 0·75, 0·85 and 0·9) and compared to the original ensemble of 60 structures calculated with $s_{vdw} = 0{\cdot}8$. In addition, a set of 20 structures was calculated using the hard sphere van der Waals radii employed by the programs DISMAN (Braun & Go, 1985) and DIANA (Güntert *et al.*, 1991). The values of these van der Waals radii are listed in Table 2 for comparison with those employed in the CHARMM PARAM19/PARAM20 empirical energy function (Brooks *et al.*, 1983; Reiher, 1985).

(f) *Evaluation of relaxation matrix refinement*

To evaluate the performance of relaxation matrix refinement on the accuracy and precision of the resulting ensemble of structures, a series of simulated annealing calculations using XPLOR 3.0 (Brünger, 1992*a*; Nilges *et al.*, 1991) were carried out in which the interproton distance restraints term in the target function was replaced by one directly describing the NOE intensities using the method of Yip & Case (1991). The NOE relaxation target function, F_{rel}, is given by:

$$F_{rel} = \sum \begin{cases} k_{rel}\{[s_{rel}(I_{io}-\Delta_i)]^{1/6} - I_{ic}^{1/6}\}^2, & \text{if } I_{ic}^{1/6} < [s_{rel}(I_{io}-\Delta_i)]^{1/6} \\ 0, & \text{if } [s_{rel}(I_{io}-\Delta_i)]^{1/6} \le I_{ic}^{1/6} \le [s_{rel}(I_{io}+\Delta_i)]^{1/6} \\ k_{rel}\{I_{ic}^{1/6} - [s_{rel}(I_{io}+\Delta_i)]^{1/6}\}^2, & \text{if } I_{ic}^{1/6} > [s_{rel}(I_{io}+\Delta_i)], \end{cases} \quad (6)$$

where I_{io} and I_{ic} are the observed and calculated NOE intensities, respectively, Δ_i is the error in the observed NOE intensity, s_{rel} is a calibration factor to scale the observed NOE intensities to the calculated ones and is simply determined by the ratio of all the calculated and observed intensities, and k_{rel} is the NOE relaxation force constant.

Model NOE intensities corresponding to the 854 structurally useful NOEs assigned experimentally (i.e. the NOE intensities corresponding to the 854 interproton distance restraints used in the preceding calculations), were calculated for the restrained minimized average structure $(\overline{SA})_{r854}$ and for one of the SA structures, denoted SA_x, from the original ensemble of 60 SA structures, using a mixing time of 150 ms, $\langle r^{-3}\rangle^{-1/3}$ averaging for methyl groups, uniform isotropic tumbling with a rotational correlation time of 3·3 ns, and no distance cutoff for the computation of relaxation pathways. The errors specified for the NOE intensities were 5%, 20% and 50% for strong (intensity >0·1, normalized to the theoretical diagonal intensity), medium (0·1 ≥ intensity ≥ 0·01) and weak (intensity < 0·01) NOEs, respectively. A series of simulated annealing refinements starting from the SA structures were carried out against these model NOE intensity data sets (ten for the data set derived from $(SA)_{r854}$ and six for the data set derived from one of the SA structures). The protocol employed comprised three steps: (1) 0·25 ps dynamics (with a time step of 1 fs) at 1000 K in which the force constant k_{rel} was increased from 51·2 up to a maximum value of 512 by doubling its value every 50 fs; (2) 1 ps of simulated annealing with k_{rel} set to 512 during which time the temperature was gradually decreased from 1000 K to 100 K; and (3) 125 cycles of Powell minimization with k_{rel} set to 512. The values of the force constants for the other terms in the target

function (i.e. covalent geometry, van der Waals repulsion, and torsion angle and hydrogen bonding restraints) were held constant at the same final values used in the simulated annealing protocol with interproton distance restraints described above; similarly, the van der Waals radius scale factor s_{vdw} for the quartic van der Waals repulsion term (eqn (4)) was set to 0·8 throughout. A cutoff of 4·5 Å was used in the computation of the relaxation matrix, and F_{rel} was recalculated every time a proton in the NOE restraints list moved by more than 0·03 Å.

To assess the agreement of the calculated and target NOE intensities, two R factors, R_1 and $R_{1/6}$, given by:

$$R_n = \sum \begin{cases} \{[s_{rel}(I_{io}-\Delta_i)]^n - I_{ic}^n\}/(s_{rel}I_{io})^n, & \text{if } I_{ic}^n < [s_{rel}(I_{io}-\Delta_i)]^n \\ 0, & \text{if } [s_{rel}(I_{io}-\Delta_i)]^n \le I_{ic}^n \le [s_{rel}(I_{io}+\Delta_i)]^n \\ \{I_{ic}^n - [s_{rel}(I_{io}+\Delta_i)]^n\}/(s_{rel}I_{io})^n, & \text{if } I_{ic}^n > [s_{rel}(I_{io}+\Delta_i)]^n, \end{cases} \quad (7)$$

were computed with $n = 1$ and $n = 1/6$. The latter corresponds to the R-factor suggested by Thomas *et al.* (1991).

(g) *Definition of precision and accuracy of calculated structures*

A key aim of the present analysis is to examine the effects of a variety of parameters on both the precision and accuracy of the resulting ensemble of structures. While it is tempting to regard precision and accuracy as identical, they are, in fact, quite distinct, even if to some extent they are interdependent. The precision of an NMR structure determination indicates how close the calculated structures are to each other and is given by the value of the average atomic r.m.s. deviation of the individual structures in a given ensemble from the overall mean co-ordinate positions for the ensemble. The accuracy of an NMR structure determination, on the other hand, represents how close the calculated structures are to the "true" mean structure and is therefore given by the average atomic r.m.s. deviation of the structures in a given ensemble from the "true" mean structure. In an experimental structure determination, the true mean structure is, of course, unknown so that it is impossible to obtain a direct measure of accuracy. In the present case, however, the model interproton distance data sets are derived from an ensemble of 60 simulated annealing structures whose average, $\overline{SA}_{854}$, therefore represents the true mean structure. In all the calculations presented below using interproton distance restraints, this mean structure is used as the reference structure. In the calculations using model NOE intensities and relaxation matrix refinement, the structure used to calculate the model NOE intensities represents the true structure.

In addition to the accuracy and precision of an ensemble of structures, we also consider the accuracy of the calculated mean co-ordinates which is defined by the r.m.s. difference between the mean co-ordinates of a given ensemble of structures and the true mean.

One other concept, namely that of intrinsic accuracy, should also be discussed. In real life, the structure of a protein, either in solution or in the crystal state, is not static but dynamic. Consequently, it can only be represented by an ensemble of structures which can be described by mean and atom-based standard deviations. Hence, non-mobile regions of the structure will have a high intrinsic accuracy, whereas mobile regions will be of low intrinsic accuracy. This concept imposes an absolute limit on the attainable accuracy and precision of an experimental structure determination, as it is evident that accuracies or precisions that are higher than the intrinsic accuracy have no physical significance.

3. Results

(a) *General structural statistics*

A key aspect of any NMR structure determination is that the ensemble of calculated structures should satisfy the experimental NMR restraints, exhibit good non-bonded contacts and display very small deviations from idealized covalent geometry. All the calculated structures satisfy the above criteria, indicating that they have located the global minimum region of the target function employed in their computation. Thus, the average r.m.s. deviations from ideality are $\le 0{\cdot}003$ Å for bonds, $\le 2°$ for angles and $\le 0{\cdot}5°$ for improper torsions (i.e. planarity and chirality restraints); the average r.m.s. deviations from the experimental torsion (ϕ, ψ and χ_1) and hydrogen-bonding restraints range from 0·1° to 0·4° and from 0·001 Å to 0·05 Å, respectively; and none of the structures exhibit violations $> 0{\cdot}5$ Å with respect to the experimental interproton distance restraints used in their calculation. Finally, for all structures calculated with the van der Waals radius scale factor, s_{vdw}, set to 0·8 (cf. eqn (4)), the values of the quartic van der Waals repulsion term F_{repel} and the Lennard–Jones energy (calculated after the fact using the CHARMM PARAM19/PARAM20 empirical energy function) range from 4 to 11 kcal·mol^{-1} and from -186 to -225 kcal·mol^{-1}, respectively.

(b) *Effect of number, precision and accuracy of interproton distance restraints on the precision and accuracy of the resulting structures*

Superpositions of calculated structures obtained with the different number, precision and accuracy of interproton distance restraints, are shown in Figure 2, and the corresponding values for their precision

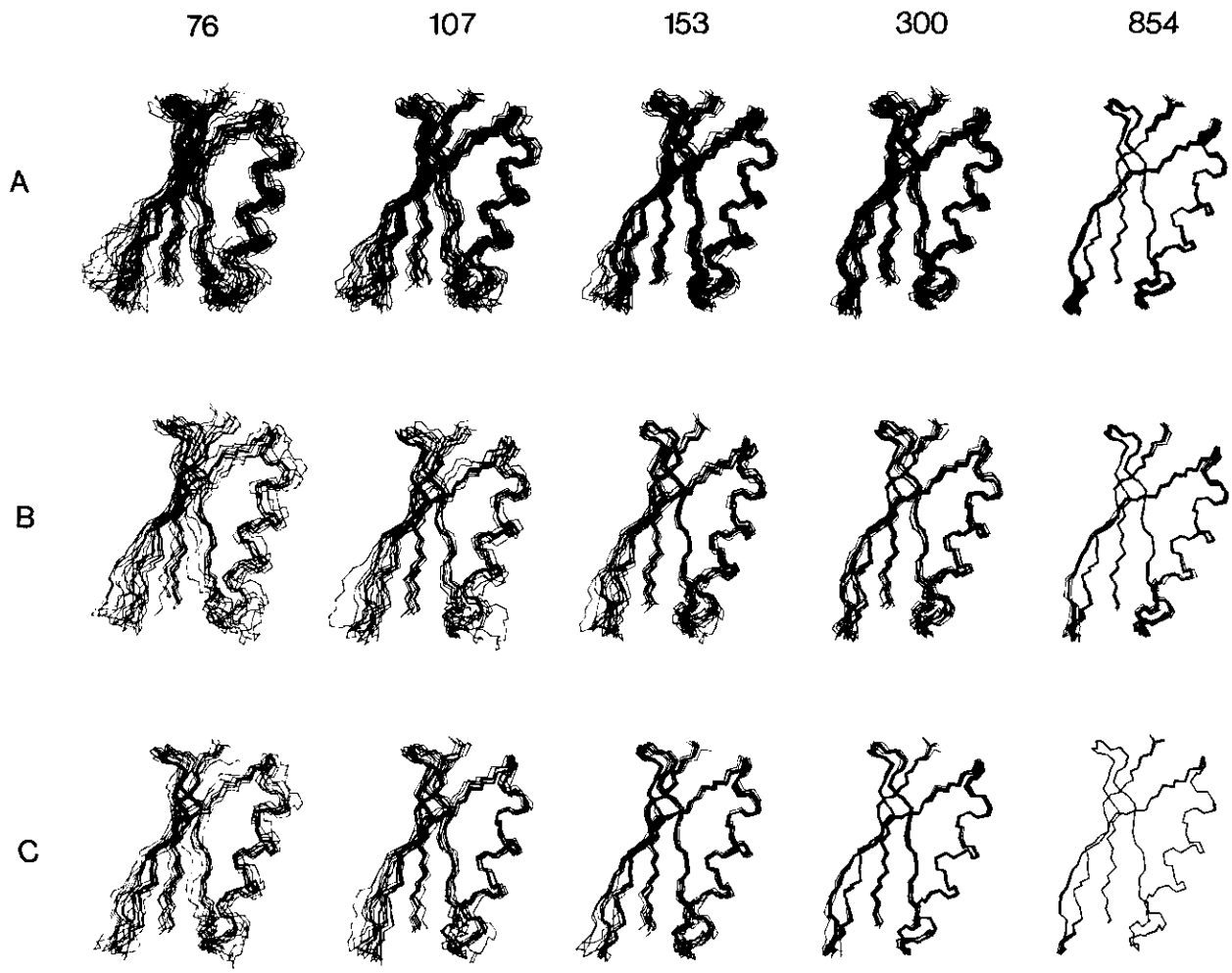

Figure 2. Best fit superpositions of backbone (N, C^{α}, C) atoms of the structures calculated with different numbers and types (approximate, precise or accurate) of interproton distance restraints. The number of interproton distance restraints are indicated above the Figure. A, Structures calculated with approximate restraints (loose square-well potential; B, with precise restraints (restrictive square-well potential); and C, with accurate restraints (harmonic potential). In the case of the ensemble calculated with the approximate restraints, there are 20 structures superimposed for the ensembles obtained with 76, 107, 153 and 300 restraints, and 60 structures are superimposed for the ensemble obtained with 854 restraints; in the case of the ensemble calculated with the precise or accurate restraints, 10 structures are superimposed, with the exception of those calculated with 76 and 107 precise restraints, where 9 structures are superimposed.

and accuracy are plotted in Figure 3 and summarized in Table 3. These data permit one to draw the following conclusions.

(1) The approximate global fold can be determined, albeit with both low precision and accuracy, with as few as an average of ~1·4 restraints per residue. Thus, for example, the precision and accuracy of the structures calculated with 76 approximate interproton distance restraints, have values of 1·2 Å and 2·0 Å, respectively (Table 3). In practice, however, at least twice as many restraints would probably be required. The reason for this is that the ten subsets of 76 interproton distance restraints originate from a much larger set of 854 restraints, and therefore comprise NOE restraints that could not be unambiguously assigned at such an early stage of a structure determination. Further, the restraints list includes stereospecific assignments, torsion angle restraints and hydrogen bonding restraints which, likewise, would not be available at such an early stage.

(2) For a given number of interproton distance restraints, there is only a small difference in either the precision or accuracy of the resulting structures computed with approximate or precise restraints (Table 3). The precision of the structures calculated with accurate restraints, on the other hand, is significantly higher than those calculated with approximate restraints (Table 3). However, it should be borne in mind that, in a real experimental case, irrespective of the accuracy of the measured NOE intensities, it is not feasible to obtain accurate interproton distance restraints, owing to ill-determinacy of spin-diffusion pathways, as well as systematic errors arising from internal motion (Clore & Gronenborn, 1989*b*). (The former arises when a particular NOE is dominated by indirect cross-relaxation so that the direct cross-relaxation

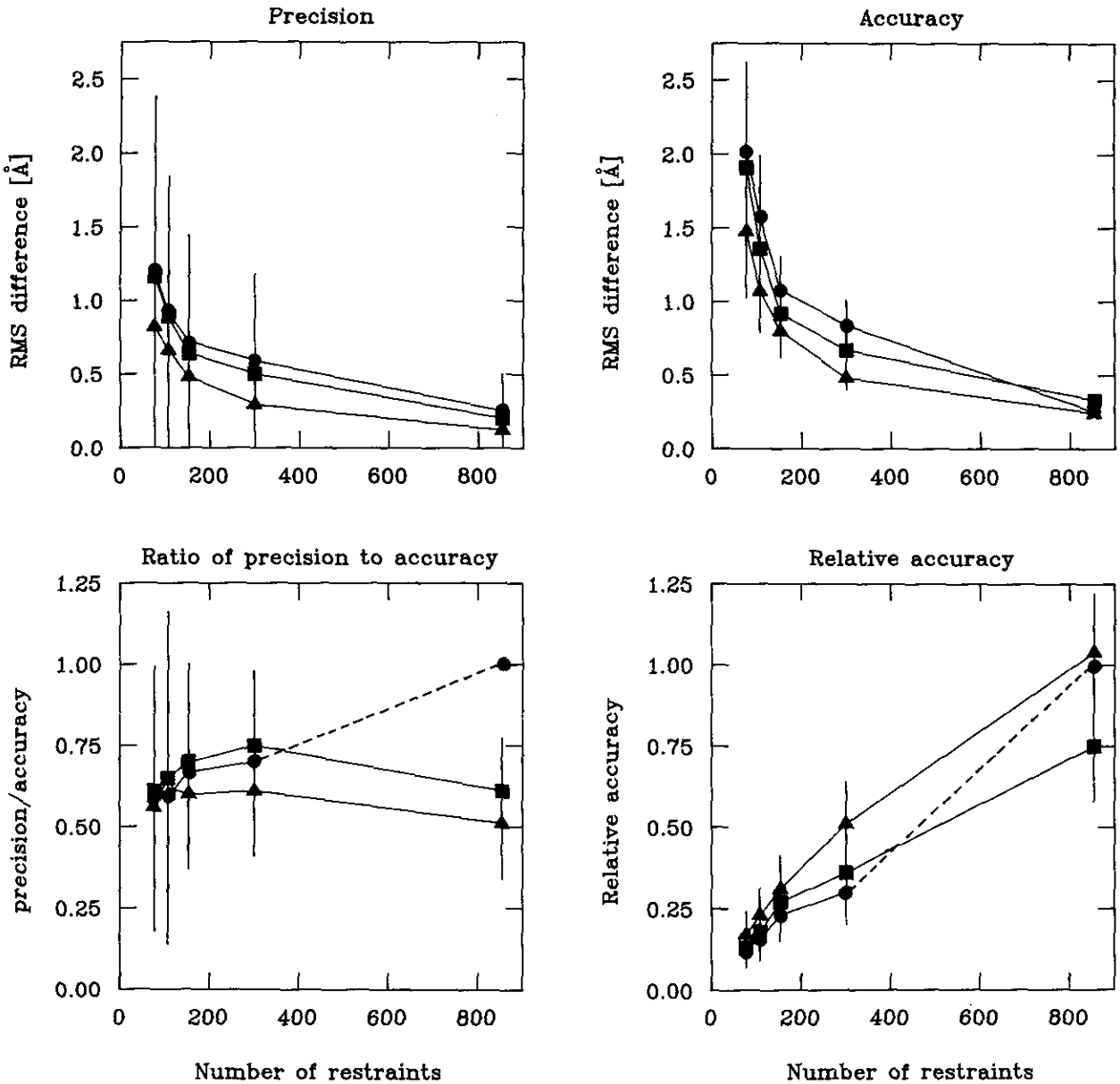

Figure 3. Variation of the precision, the accuracy, the ratio of precision to accuracy and the relative accuracy for the backbone (N, C^{α}, C) atoms of the ensemble of structures calculated with approximate (●), precise (■) and accurate (▲) interproton distance restraints as a function of the number of interproton distance restraints. The symbols represent the mean values and the vertical bars are their standard deviations. As the ensemble of 60 structures calculated with the complete set of 854 approximate restraints is used as a reference in the current study, the ratio of precision to accuracy and the relative accuracy of this ensemble of structure is by definition 1. Hence, the use of broken lines to connect the values of the ratio of precision to accuracy and of the relative accuracy for the ensemble of structures calculated with 300 approximate interproton distance restraints to those calculated with 854 approximate interproton distance restraints.

rate is ill-determined; consequently, an upper limit of the distance is determined purely by the limits imposed by covalent geometry, while the lower limit is determined by the balance between the direct and indirect cross-relaxation rates.) Further, as discussed in Calculation Strategy, section (b), the precise restraints employed in these calculations are significantly more precise than the highest precision that can possibly be achieved using, for example, iterative relaxation matrix analysis.

(3) The most dramatic improvement in both precision and accuracy of the calculated structures results from increasing the number, rather than either the precision or accuracy, of the interproton distance restraints (Figs 2 and 3; Table 3). The reason for this is that the extent of redundancy in a data set consisting of less than about ten restraints per residue is rather small. Hence, it is not surprising to find that while the structures calculated with a subset of the interproton distance restraints satisfy the restraints used to calculate these structures (i.e. no violations >0·5 Å), they do not satisfy the remainder of the interproton distance restraints, as evidenced by numerous viola-

Table 3

Effect of number, precision and accuracy of interproton distance restraints on the precision and accuracy of the ensemble of calculated structures for the 56 residue IgG binding domain of streptococcal protein G

Number of interproton distance restraints	Approximate restraints	Precise restraints	Accurate restraints
A. *Atomic r.m.s. deviation: precision/accuracy (Å)*			
Backbone atoms†			
76	1·19 ± 0·45/2·02 ± 0·60	1·16 ± 0·22/1·91 ± 0·57	0·82 ± 0·30/1·48 ± 0·45
107	0·93 ± 0·19/1·57 ± 0·42	0·89 ± 0·34/1·36 ± 0·54	0·66 ± 0·17/1·07 ± 0·28
153	0·72 ± 0·14/1·08 ± 0·23	0·64 ± 0·13/0·92 ± 0·21	0·48 ± 0·08/0·80 ± 0·18
300	0·59 ± 0·10/0·84 ± 0·17	0·50 ± 0·07/0·67 ± 0·11	0·29 ± 0·05/0·48 ± 0·08
854	0·25 ± 0·03/0·25 ± 0·03	0·20 ± 0·03/0·33 ± 0·04	0·12 ± 0·03/0·24 ± 0·02
All atoms			
76	1·56 ± 0·46/2·38 ± 0·60	1·50 ± 0·20/2·27 ± 0·48	1·18 ± 0·28/1·78 ± 0·42
107	1·28 ± 0·17/1·89 ± 0·39	1·19 ± 0·34/1·66 ± 0·51	0·99 ± 0·16/1·40 ± 0·24
153	1·12 ± 0·13/1·45 ± 0·22	0·98 ± 0·11/1·25 ± 0·19	0·81 ± 0·07/1·09 ± 0·16
300	0·93 ± 0·08/1·17 ± 0·16	0·83 ± 0·09/1·02 ± 0·09	0·68 ± 0·06/0·85 ± 0·10
854	0·65 ± 0·05/0·65 ± 0·05	0·65 ± 0·06/0·73 ± 0·04	0·51 ± 0·03/0·61 ± 0·03
All ordered atoms‡			
76	1·40 ± 0·46/2·24 ± 0·59	1·35 ± 0·20/2·10 ± 0·53	1·01 ± 0·29/1·64 ± 0·43
107	1·14 ± 0·18/1·78 ± 0·40	1·05 ± 0·35/1·51 ± 0·55	0·83 ± 0·17/1·22 ± 0·29
153	0·91 ± 0·16/1·27 ± 0·25	0·82 ± 0·13/1·08 ± 0·22	0·62 ± 0·08/0·91 ± 0·17
300	0·74 ± 0·09/0·97 ± 0·17	0·64 ± 0·07/0·81 ± 0·11	0·44 ± 0·06/0·61 ± 0·08
854	0·39 ± 0·03/0·39 ± 0·03	0·37 ± 0·04/0·45 ± 0·04	0·25 ± 0·03/0·36 ± 0·02
B. *Ratio of precision to accuracy*			
	backbone†/all atoms/all ordered atoms‡	backbone†/all atoms/all ordered atoms‡	backbone†/all atoms/all ordered atoms‡
76	0·59 ± 0·40/0·66 ± 0·36/0·63 ± 0·37	0·61 ± 0·30/0·66 ± 0·23/0·64 ± 0·26	0·56 ± 0·38/0·66 ± 0·31/0·62 ± 0·34
107	0·59 ± 0·28/0·67 ± 0·23/0·64 ± 0·25	0·65 ± 0·51/0·72 ± 0·43/0·70 ± 0·49	0·62 ± 0·32/0·71 ± 0·24/0·68 ± 0·30
153	0·67 ± 0·27/0·77 ± 0·21/0·72 ± 0·27	0·70 ± 0·30/0·78 ± 0·21/0·76 ± 0·28	0·60 ± 0·23/0·74 ± 0·17/0·68 ± 0·22
300	0·70 ± 0·26/0·79 ± 0·18/0·76 ± 0·23	0·75 ± 0·23/0·81 ± 0·16/0·79 ± 0·19	0·61 ± 0·20/0·80 ± 0·16/0·72 ± 0·19
854	1§/1§/1§	0·61 ± 0·16/0·89 ± 0·13/0·82 ± 0·17	0·51 ± 0·17/0·84 ± 0·09/0·69 ± 0·12
mean	0·64 ± 0·30§/0·72 ± 0·25§/0·69 ± 0·28§	0·66 ± 0·30/0·77 ± 0·23/0·74 ± 0·28	0·58 ± 0·26/0·75 ± 0·19/0·68 ± 0·23
C. *Relative accuracy*			
	backbone†/all atoms/all ordered atoms‡	backbone†/all atoms/all ordered atoms‡	backbone†/all atoms/all ordered atoms‡
76	0·12 ± 0·05/0·27 ± 0·09/0·17 ± 0·06	0·13 ± 0·05/0·29 ± 0·08/0·19 ± 0·06	0·17 ± 0·07/0·37 ± 0·11/0·24 ± 0·08
107	0·16 ± 0·06/0·34 ± 0·10/0·22 ± 0·07	0·18 ± 0·09/0·39 ± 0·15/0·26 ± 0·11	0·23 ± 0·08/0·46 ± 0·12/0·32 ± 0·10
153	0·23 ± 0·08/0·45 ± 0·10/0·31 ± 0·08	0·27 ± 0·09/0·52 ± 0·12/0·36 ± 0·11	0·31 ± 0·10/0·60 ± 0·13/0·36 ± 0·08
300	0·30 ± 0·10/0·51 ± 0·12/0·40 ± 0·10	0·36 ± 0·10/0·64 ± 0·11/0·48 ± 0·10	0·51 ± 0·13/0·76 ± 0·15/0·64 ± 0·13
854	1§/1§/1§	0·75 ± 0·17/0·89 ± 0·12/0·87 ± 0·14	1·04 ± 0·18/1·07 ± 0·13/1·08 ± 0·14

D. *Accuracy of mean co-ordinates (r.m.s. difference between ensemble mean and SA_{854})*

	backbone†	all atoms	all ordered atoms‡	backbone†	all atoms	all ordered atoms‡	backbone†	all atoms	all ordered atoms‡
76	1·68	1·84	1·78	1·61	1·76	1·69	1·27	1·37	1·33
107	1·32	1·42	1·40	1·12	1·23	1·17	0·87	1·00	0·92
153	0·82	0·94	0·88	0·67	0·79	0·73	0·66	0·75	0·68
300	0·61	0·74	0·66	0·46	0·60	0·50	0·38	0·52	0·42
854	0	0	0	0·22	0·34	0·26	0·21	0·35	0·26

The precision is given by the average atomic r.m.s. deviation of the individual structures of a given ensemble from the ensemble average co-ordinates; the accuracy is given by the average atomic r.m.s. deviation of the individual structures within a given ensemble to the reference mean structure, $\overline{SA}_{854}$, obtained from the 60 individual simulated annealing structures calculated with the 854 approximate interproton distance restraints and $s_{vdw} = 0{\cdot}80$. The relative accuracy is given by the ratio of the accuracy of the structures in a given ensemble to that of the reference ensemble of 60 structures calculated with the 854 approximate interproton distance restraints and $s_{vdw} = 0{\cdot}80$ (i.e. to PDB accession code number 2GB1).

† The atoms included for the backbone atoms are the N, C^{α} and C atoms.

‡ The disordered surface side-chains that are excluded are: Met1 from the C^{β} position onward, Lys4 from C^{δ}, Lys10 from C^{γ}, Lys13 from C^{δ}, Glu15 from C^{γ}, Glu19 from C^{γ}, Lys28 from C^{γ}, Lys31 from C^{δ}, Gln32 from C^{δ}, Glu42 from C^{δ} and Glu56 from C^{δ} (Gronenborn *et al.*, 1991).

§ The atomic r.m.s. deviations for the 60 structures calculated with the 854 approximate interproton distance restraints and $s_{vdw} = 0{\cdot}8$ represent the reference ensemble whose mean structure is SA_{854}. Hence, their precision and accuracy are by definition identical.

tions >1 Å, including a number >4 Å. Naturally, the larger the subset of restraints used in a given calculation, the smaller the number of violations with respect to the unused restraints, be they approximate, precise or accurate.

(4) The ratio of precision to accuracy for an ensemble of structures appears, in general, to be approximately independent of either the number, the precision or the accuracy of the interproton distance restraints (Fig. 3 and Table 3B). This ratio, however, does depend on the intrinsic accuracy of the true structure. In this series of model calculations, the intrinsic accuracy is by definition equal to both the precision and accuracy of the 60 structures calculated with the 854 approximate interproton distance restraints, as these comprise the basis set for all the model interproton distance restraints. In this particular case, and in all likelihood in general, the intrinsic accuracy of the backbone is greater than that for all atoms, as the latter comprises, for example, disordered surface side-chains, which necessarily have low intrinsic accuracy. The value of the ratio of precision to accuracy is inversely related to the intrinsic accuracy. Hence, the higher the intrinsic accuracy, the lower the ratio of ensemble precision to ensemble accuracy of the calculated structures. This is manifested by a lower value of the ratio of precision to accuracy for the backbone (~0·6) compared to that for all atoms (~0·75), with an intermediate value for all atoms excluding those of disordered side-chains (~0·7).

(5) The accuracy of the mean co-ordinates is invariably better than that of any of the individual structures in a given ensemble (cf. compare Tables 3A and D). In other words, the r.m.s. difference between the mean co-ordinates of a given ensemble and the true mean is always smaller than the r.m.s. difference between the individual structures of a given ensemble and the true mean. This parallels previous observations made in both model calculations (Clore *et al.*, 1986*b*) and in comparisons between NMR and X-ray structures (Clore *et al.*, 1987*a*,*b*; Clore & Gronenborn, 1991*c*,*d*,*e*; Billeter *et al.*, 1989, 1992). When the ratio of precision to accuracy of the ensemble of structures exceeds a value of ~0·75, the r.m.s. difference between the ensemble mean and the true mean is smaller than the r.m.s. difference between the individual structures of the ensemble and the ensemble mean. Hence, under these conditions, the true mean lies within the ensemble of calculated structures. The dependence of the accuracy of the mean co-ordinates as a function of the precision of the ensemble is shown in Figure 4. For an average ensemble precision >0·6 Å, the dependence of the mean co-ordinates on the ensemble precision is approximately linear. As the ensemble precision is increased beyond ~0·6 Å, the dependence is asymptotic, reaching a limiting value of ~0·1 Å for backbone atoms, all atoms and all ordered atoms. The curves obtained for the structures calculated with the approximate (excluding the reference ensemble) and precise interproton distance restraints are completely superimposable. The curves obtained for the structures calculated with the accurate interproton distance restraints, on the other hand, are displaced to the left. Hence, for a given level of ensemble precision, the accuracy of the mean co-ordinates obtained for an ensemble of structures calculated with approximate or precise interproton distance restraints is actually more accurate than that of the mean co-ordinates obtained from an ensemble of structures calculated with accurate interproton distance restraints. This is presumably due to a slightly different balance of forces in the target function for these three cases. Further, for a given level of ensemble precision, the accuracy of the mean co-ordinates is greater for all atoms than for all ordered atoms which, in turn, is greater than that for the backbone atoms. This is related to the concept of intrinsic accuracy discussed above.

(6) Both the precision and accuracy of the structures is directly correlated to their radii of gyration (Fig. 5). Thus, the low precision, low accuracy structures calculated with a small number of restraints are expanded relative to the high precision, high accuracy structures calculated with the full complement of restraints. This can also be appreciated visually from the various superpositions of structures shown in Figure 2. This observation is not too surprising as the only attractive forces present in the target function are those associated with the potential for the interproton distance restraints. Hence, the fewer the number of interproton distance restraints, the smaller the contribution of the attractive forces to the target function.

(7) The maximum accuracy achievable is about 0·25 Å for the backbone atoms, 0·6 Å for all atoms and 0·4 Å for ordered side-chains (Table 3). Thus, for example, even though the precision of the backbone co-ordinates for the structures calculated with the 854 accurate interproton distance restraints (0·12 Å) is almost double that of the reference ensemble calculated with the 854 approximate restraints (0·25 Å), the accuracy of the two sets of structures is identical (0·25 Å). (Note that as the structures calculated with the 854 approximate interproton distance restraints comprise the reference ensemble, their precision and accuracy are by definition identical.) Similar results are observed for all atoms, as well as all ordered atoms. It is also noteworthy that despite the fact that the precision of the ensemble of structures calculated with the 854 precise interproton distance restraints is approximately the same as that calculated with the 854 approximate interproton distance restraints, the accuracy of the former is a little lower than that of the latter. Nevertheless, with the exception of the backbone atoms for the ensemble of structures calculated with the 854 accurate restraints, the true mean lies within the ensemble of structures calculated with either 854 precise or accurate restraints. These results, in all likelihood, represent the absolute limits on both accuracy and precision that can be obtained in practice as this data set

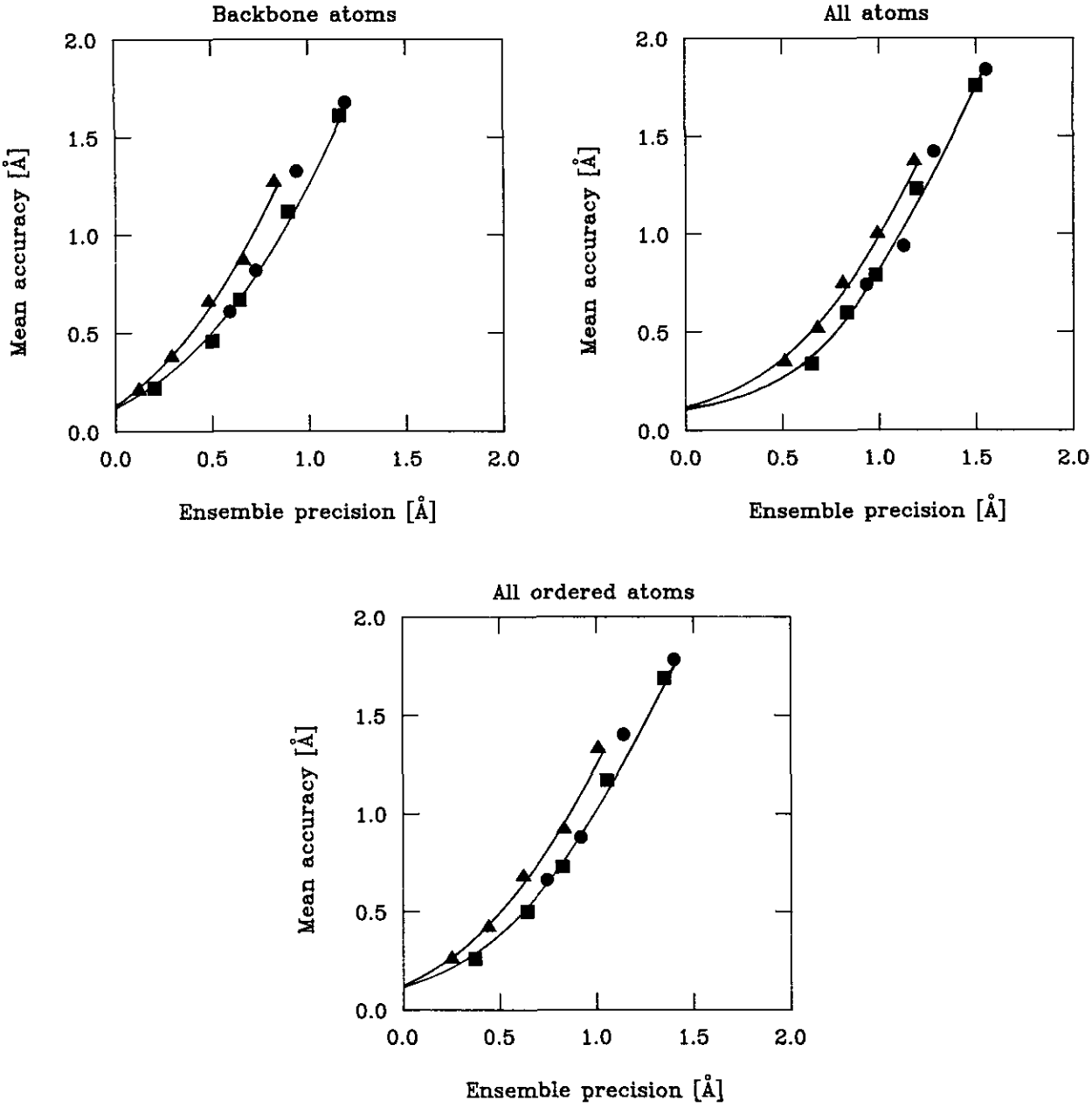

Figure 4. Dependence of the accuracy of the mean co-ordinates on ensemble precision for structures calculated with approximate (●), precise (■) and accurate (▲) interproton distance restraints. The accuracy of the mean co-ordinates has a limiting value of ~0·13 Å for backbone atoms, all atoms and all ordered atoms. (Note that the plots do not include data for the reference ensemble calculated with the complete set of 854 approximate interproton distance restraints; for a definition of all ordered atoms, see footnote ‡ to Table 3.)

comprises all the structurally useful NOEs that are observed experimentally. Moreover, analysis of the data indicates that both the accuracy and precision follow an approximately x^{-n} dependence on the number of distances x, where n varies from ~0·6 to ~0·8. Hence, any significant improvement over the results obtained with the set of 854 interproton distance restraints (corresponding to ~15 restraints per residue with ~9 restraints per residue involving unique proton pairs) would require an approximate doubling of the number of interproton distance restraints.

(c) *Effect of full NOE relaxation matrix refinement on the precision and accuracy of the calculated structures*

Although it is not feasible to obtain accurate interproton distances from NOE data, it is potentially possible to obtain accurate measurements of NOE intensities. Consequently, it is of interest to assess the effect of direct refinement against NOE intensities on the accuracy and precision of the resulting structures. Two series of calculations were carried out, using model NOE intensities corre-

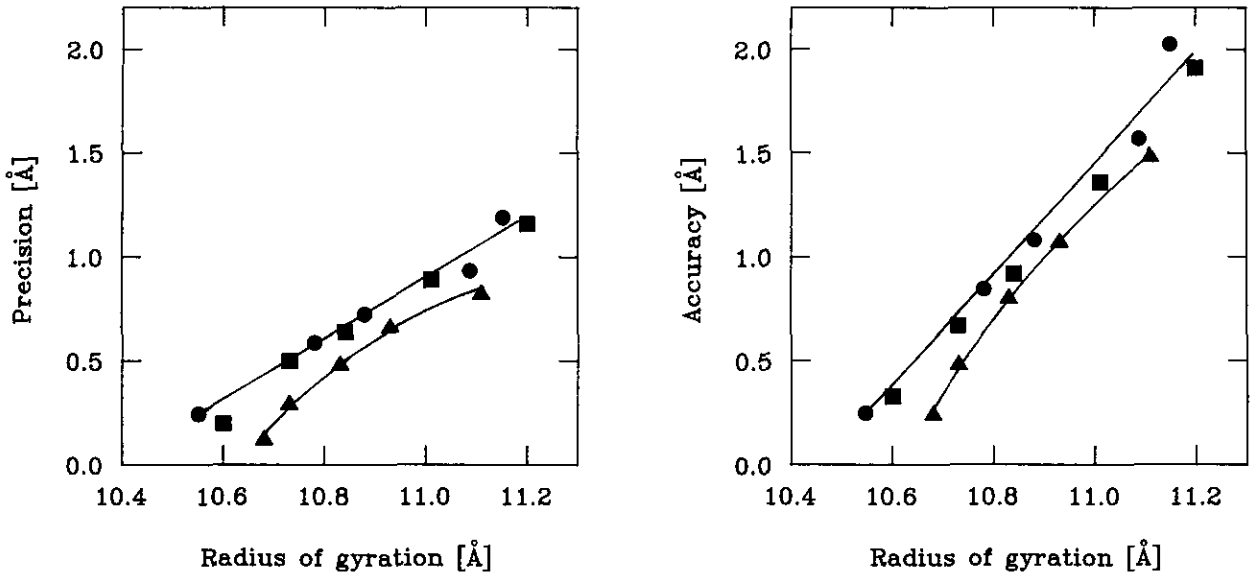

Figure 5. Variation of the precision and accuracy for the backbone (N, C^{α}, C) atoms of the ensemble of structures calculated with approximate (●), precise (■) and accurate (▲) interproton distance restraints as a function of their radii of gyration.

sponding to the 854 interproton distance restraints. In the first series the NOE intensities were derived from the restrained minimized average structure $(\overline{SA})_{r854}$, while in the second they were obtained from one of the SA structures, denoted as SA_x, calculated with the 854 approximate interproton distance restraints. In both cases the NOE intensities represent idealized intensities as they are calculated assuming a rigid molecule and hence do not include any complications that could arise in practice from internal motions. They do, however, include likely experimental errors in peak integration as they are represented by square-well potentials with errors of 5, 20 and 50% for strong, medium and weak NOEs, respectively (see Calculational Strategy, section (e)). A superposition of the backbone atoms of the refined structures from the first series of calculations is shown in Figure 6, together with a superposition of the mean structure after relaxation matrix refinement with the restrained minimized average structure $(\overline{SA})_{r854}$. A summary of the *R*-factors and r.m.s. differences before and after relaxation matrix refinement is provided in Tables 4 and 5, respectively.

In both sets of calculations, the structures generated by the full relaxation matrix refinement

Table 4

Relaxation matrix refinement R*-factors for the calculated structures of the 56 residue IgG binding domain of streptococcal protein G*

Structure	$R_{1/6}$	R_1
A. *Model NOE intensities from* $(SA)_{r854}$		
Before relaxation matrix refinement $\langle SA \rangle$ ($N = 10$)	0·0051 ± 0·0011	0·070 ± 0·021
After relaxation matrix refinement $\langle RR \rangle$ ($N = 10$)	0·0013 ± 0·0003	0·020 ± 0·004
B. *Model NOE intensities from structure* SA_x		
Before relaxation refinement $\langle SA \rangle_{j \neq x}$ ($N = 6$)	0·0050 ± 0·0010	0·067 ± 0·017
After relaxation refinement $\langle RR2 \rangle$ ($N = 6$)	0·0031 ± 0·0006	0·029 ± 0·005

The structures are obtained by simulated annealing relaxation matrix refinement against model NOE intensities corresponding to the 854 approximate interproton distance restraints (PDB accession code no. R1GB1MR). ⟨RR⟩ represent the 10 structures calculated using model NOE intensities derived from $(\overline{SA})_{r854}$ (PDB accession code no. 1GB1); ⟨RR2⟩ represent the 6 structures calculated using model NOE intensities derived from one of the 60 structures, denoted as SA_x, obtained with the 854 approximate interproton distance restraints (PDB accession code no. 2GB1). The definition of the two *R*-factors, $R_{1/6}$ and R_1, is given by eqn (7). The model NOE intensities are represented by square-well potentials (eqn. (6)) with errors of 5, 20 and 50% for strong medium and weak NOEs, respectively (see Calculational Strategy, section (e)).

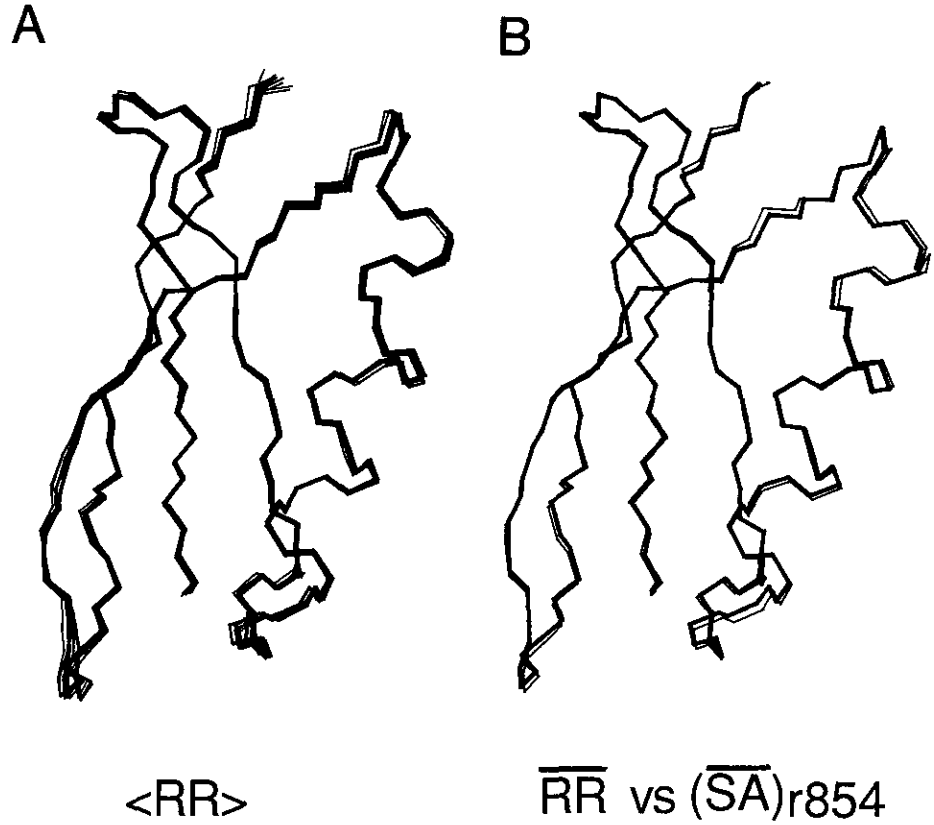

Figure 6. A, Superposition of the backbone (N, C^{α}, C) atoms of the 10 structures obtained by simulated annealing relaxation matrix refinement against the calculated NOE intensities (corresponding to the 854 structurally useful NOEs assigned experimentally) derived from the restrained minimized mean structure $(\overline{SA})_{r854}$. B, Superposition of the backbone (N, C^{α}, C) atoms of the mean co-ordinates of the 10 relaxation matrix refined structures (thin line) and the restrained minimized mean structure $(\overline{SA})_{r854}$ (thick line).

display good covalent geometry and non-bonded contacts, as well as very small deviations from the torsion angle and hydrogen bonding restraints (cf. section (a), above). In addition, the agreement with the model NOE intensities improved significantly. Thus, in the case of the calculations with the model NOE intensities derived from $(\overline{SA})_{r854}$, the $R_{1/6}$ and R_1 *R*-factors decreased from values of 0·5% and 7%, respectively, before refinement to 0·13% and 2%, respectively, after refinement (Table 4). Interestingly, however, the number of interproton distance violations with respect to the complete set of 854 approximate or precise interproton distance restraints is larger for the structures (⟨RR⟩) after relaxation matrix refinement than for either the ten SA structures before refinement or the restrained minimized average structure $(\overline{SA})_{r854}$. Thus, whereas the ten SA structures prior to relaxation matrix refinement exhibit no interproton distance violations >0·3 Å, the ten RR structures after relaxation matrix refinement display an average of 14·4±3·1, 4·9±1·5 and 0·2±0·4 violations in the range 0·3 to 0·5 Å, 0·5 to 1·0 Å and 1·0 to 2·0 Å, respectively. This reflects the ill-determinacy of some of the relaxation pathways, particularly with regard to the balance between direct and indirect cross-relaxation (Clore & Gronenborn, 1989*b*). Moreover, it should be noted that the starting SA structures in both cases, show very good agreement with the model NOE intensities, providing further proof of the small standard deviations in the vectors corresponding to the 854 interproton restraints (cf. Fig. 1 and Table 1).

The calculations carried out with the model NOE intensities derived from $(\overline{SA})_{r854}$ reveal a surprising observation. Namely, while the precision of the structures following relaxation matrix refinement is increased significantly, there is no improvement in accuracy (Table 5A). Thus, for example, the precision of the backbone co-ordinates improves from 0·27 Å before refinement to 0·15 Å following relaxation matrix refinement, while the accuracy of the backbone co-ordinates actually decreases slightly from 0·27 Å to 0·31 Å. Further, a comparison of the values for the precision of the ensemble with the accuracy of the mean co-ordinates, indicates that in the case of the backbone atoms, the true structure (i.e. $(SA)_{r854}$) actually lies outside the calculated ensemble of relaxation matrix refined structures (cf. Table 5A and 5C). In the case of the co-ordinates for either all atoms or all ordered atoms, the precision of the co-ordinates is also improved, but their accuracy remains unchanged (Table 5A).

For the calculations carried out with the model NOE intensities derived from one of the SA structures (denoted SA_x), the starting co-ordinates are, of

Table 5

Effect of relaxation matrix refinement on the precision and accuracy of the ensemble of calculated structures for the 56 residue IgG binding domain of streptococcal protein G

Structure	Atomic r.m.s. deviation: precision/accuracy (Å) (Ratio of precision to accuracy/relative accuracy) Backbone atoms†	All atoms	All ordered atoms‡
A. *Model NOE intensities from* $(SA)_{r854}$			
Before relaxation matrix refinement			
⟨SA⟩ ($N = 10$)	0·25 ± 0·03/0·27 ± 0·04 (0·93 ± 0·25/1)	0·67 ± 0·05/0·77 ± 0·05 (0·87 ± 0·12/1)	0·39 ± 0·03/0·46 ± 0·04 (0·85 ± 0·14/1)
After relaxation matrix refinement			
⟨RR⟩ ($N = 10$)	0·15 ± 0·02/0·31 ± 0·02 (0·48 ± 0·10/0·87 ± 0·19)	0·48 ± 0·05/0·68 ± 0·07 (0·71 ± 0·15/1·13 ± 0·19)	0·27 ± 0·01/0·45 ± 0·03 (0·60 ± 0·06/1·02 ± 0·16)
B. *Model NOE intensities from structure* SA_x			
Before relaxation matrix refinement			
$\langle SA \rangle_{j \neq x}$ ($N = 6$)	0·25 ± 0·02/0·39 ± 0·06 (0·64 ± 0·15/—)	0·66 ± 0·05/0·78 ± 0·04 (0·85 ± 0·11/—)	0·38 ± 0·03/0·54 ± 0·03 (0·70 ± 0·09/—)
After relaxation matrix refinement			
⟨RR2⟩ ($N = 6$)	0·16 ± 0·03/0·30 ± 0·03 (0·53 ± 0·15/—)	0·49 ± 0·03/0·79 ± 0·12 (0·62 ± 0·13/—)	0·27 ± 0·02/0·49 ± 0·06 (0·55 ± 0·11/—)
C. *Accuracy of mean co-ordinates after relaxation matrix refinement*			
$\overline{RR}$ *vs* $(\overline{SA})_{r854}$	0·28	0·49	0·36
$\overline{RR2}$ *vs* SA_x	0·26	0·64	0·41

The precision of the ensemble of ⟨RR⟩ and ⟨RR2⟩ structures is defined as the average atomic r.m.s. difference of the individual structures about their respective ensemble means. The accuracy of the ⟨RR⟩ and ⟨RR2⟩ ensemble of structures is defined as the average atomic r.m.s. difference of the individual structures from $(\overline{SA})_{r854}$ and SA_x, respectively, which represent the 2 structures, respectively, from which the target NOE intensities were calculated. The relative accuracy is only given for the ⟨RR⟩ set of structures and is defined as the ratio of the accuracy of the ⟨RR⟩ structures to that of the corresponding 10 ⟨SA⟩ structures prior to relaxation matrix refinement. Hence, the relative accuracy of the 10 ⟨SA⟩ structures is by definition 1.

† The atoms included for the backbone atoms are the N, C^{α} and C atoms.

‡ The disordered surface side-chains that are excluded are given in footnote ‡ to Table 3.

course, not centered about this structure. Hence, it is not surprising to find that the accuracy of the backbone co-ordinates is slightly increased upon refinement, although no change in accuracy is observed for the co-ordinates of either all atoms or all ordered atoms (Table 5B). More importantly, the accuracy of these co-ordinates is no different from that achieved in the calculations with the other set of model NOE intensities.

(d) *Effect of the non-bonded contact term on the precision and accuracy of the resulting structures*

Because the main source of structural information derived from NMR resides in short interproton distance restraints, other information in the form of restraints on covalent geometry and non-bonded contacts are absolutely essential to an NMR structure determination. While there is general agreement on the values of standard bond lengths and angles which vary little from one molecule to another, the representation of the non-bonded contacts is more problematic. The non-bonded contributions may be partitioned into three categories: van der Waals, electrostatic and hydrogen bonding. It is precisely these terms that differ most from one empirical energy parameter set to another (Momany *et al.*, 1974; Brooks *et al.*, 1983; Reiher, 1985; Weiner *et al.*, 1984, 1986; Nilsson & Karplus, 1986; Dauber-Osguthorpe *et al.*, 1988). In the case of an NMR structure determination, the simplest approach is to represent the non-bonded contacts solely by a repulsion term which prevents atoms from coming too close together (e.g. eqn (4)). To test the effect of this term on the resulting structures, we carried out a series of calculations in which the van der Waals radius scale factor s_{vdw} of the quartic van der Waals repulsion potential given by equation (4) was varied from 0·70 to 0·90 for the CHARMM PARAM19/PARAM20 van der Waals radii (Brooks *et al.*, 1983; Reiher, 1985) given in Table 2. The results are summarized for the backbone in Figure 7 and a similar trend is observed for all atoms and all ordered atoms.

While the precision of the co-ordinates remain essentially unchanged as s_{vdw} is increased from 0·80 to 0·90, there is a significant decrease in accuracy, and the true mean lies outside the ensemble of calculated structures. In addition, the van der Waals Lennard–Jones energy (calculated with the CHARMM PARAM19/PARAM20 empirical energy parameters) becomes more negative, decreasing

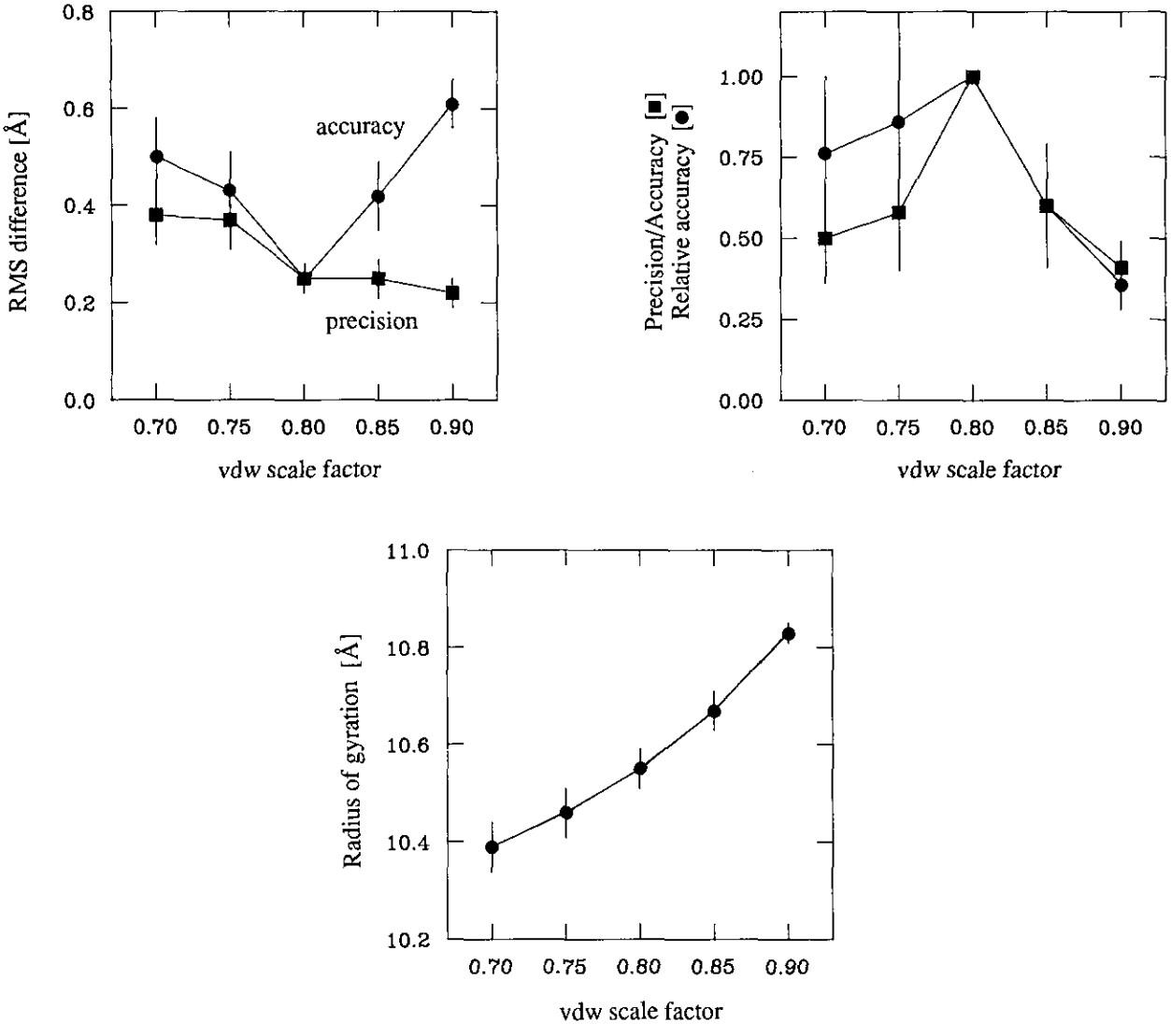

Figure 7. Variation of the precision (●), the accuracy (■), the ratio of precision to accuracy (●) and the relative accuracy (■) for the backbone (N, C^{α}, C) atoms, and variation of the radius of gyration of the ensemble of structures as a function of the van der Waals radius scale factor (cf. eqn (4)) used in their calculation. The symbols represent the mean values and the vertical bars are their standard deviations. The effective hard sphere van der Waals radius of a given atom is given by $s_{vdw} \cdot r_{vdw}$, where s_{vdw} is the van der Waals radius scale factor and r_{vdw} is the van der Waals radius employed in the CHARMM PARAM19/PARAM20 empirical energy parameters (cf. Table 2).

from $-210(\pm 7)$ kcal·mol^{-1} for $s_{vdw} = 0{\cdot}8$ to $-284(\pm 5)$ kcal·mol^{-1} for $s_{vdw} = 0{\cdot}9$, as the atoms are forced to lie further apart.

When s_{vdw} is decreased from 0·80 to 0·70, there is both a decrease in precision and accuracy, but in contrast to the results with $s_{vdw} \geq 0{\cdot}85$, the true mean still lies within the ensemble of calculated structures. The reason for the decrease in precision with decreasing values of s_{vdw} can be attributed to the increase in conformational space compatible with the target function as the effective hard sphere van der Waals radii are decreased. Also, in contrast to the results with $s_{vdw} \geq 0{\cdot}85$, the Lennard–Jones van der Waals energy becomes more positive ($-144(\pm 19)$ kcal·mol^{-1} for $s_{vdw} = 0{\cdot}75$ and $-19(\pm 34)$ kcal·mol^{-1} for $s_{vdw} = 0{\cdot}70$) as the average interatomic distances between contacting atoms decreases. Perhaps more significant is that a change in the effective hard sphere van der Waals radii by as little as 6% from their values with $s_{vdw} = 0{\cdot}8$ to those with $s_{vdw} = 0{\cdot}75$ or 0·85, results in a decrease of about 70% in the accuracy of the backbone co-ordinates. This is of considerable practical significance as variations in the van der Waals radii of this magnitude and larger are seen from one empirical energy parameter set to another. Also of interest is that the radius of gyration is proportional to s_{vdw}.

To test the effect of a set of van der Waals radii from another empirical energy parameter set, we also carried out a series of calculations using the hard sphere van der Waals radii employed by the programs DISMAN (Braun & Go, 1985) and DIANA (Güntert *et al.*, 1991). These effective radii

were derived from the ECEPP energy parameters (Momany *et al.*, 1974) and were set to values resulting in a calculated Lennard–Jones energy of 3 kcal·mol^{-1} between atom pairs (Braun & Go, 1985). The main difference between these radii and those of the PARAM19/PARAM20 energy parameters of CHARMM with $s_{vdw} = 0{\cdot}8$, lies in the values of the radii of the proton (Table 1). Thus, the effective hard sphere van der Waals radii of polar hydrogens (e.g. backbone and side-chain amide protons) are ~30% larger in the DISMAN/DIANA parameter set, while those of aliphatic and aromatic protons are approximately 15% smaller. It is worthwhile noting, in this regard, that the uncertainty in the values of the hard sphere van der Waals radii is largest for hydrogens. In addition, there are still sizeable differences of 5 to 6% in the effective hard sphere van der Waals radii employed for the nitrogen and aromatic carbon atoms. Despite these differences, the decrease in precision of the resulting structures relative to the reference structures obtained with the CHARMM PARAM19//PARAM20 radii and $s_{vdw} = 0{\cdot}8$ is small (30%, 10% and 20% for backbone atoms, all atoms and all ordered atoms, respectively). The accuracy, however, is reduced significantly by 60% for backbone atoms, 20% for all atoms and 40% for all ordered atoms. Nevertheless, the true mean still lies within the ensemble of calculated structures as the r.m.s. differences between the ensemble mean and the true mean, for backbone atoms, all atoms and all ordered atoms, are smaller than the corresponding r.m.s. values for the precision of the calculated structures. It is also worth noting that the Lennard–Jones van der Waals energy calculated with the CHARMM PARAM19/PARAM20 energy parameters is more positive for the DISMAN ensemble of structures ($-172(\pm 7)$ kcal·mol^{-1}) than for the reference structures calculated with $s_{vdw} = 0{\cdot}8$ ($-210(\pm 7)$ kcal·mol^{-1}).

It must be emphasized that these results do not in any way imply that the DISMAN radii provide a worse representation of the non-bonded interactions than the CHARMM PARAM19/PARAM20 radii with $s_{vdw} = 0{\cdot}8$, as the true and exact description of the non-bonded interactions of a protein in solution is, of course, unknown. Rather, these results provide a measure of the uncertainties in the calculated co-ordinates engendered by the uncertainties in the description of the non-bonded contacts.

4. Discussion

The results presented in this paper provide a benchmark for assessing the limits of precision and accuracy that are attainable in NMR protein structure determinations.

The main conclusions that can be derived are as follows.

(1) The most crucial determinant of both precision and accuracy is the number of interproton distance restraints (Table 3; Figs 2 and 3). Further, while large increases in precision and accuracy are observed as the number of restraints is increased to an average of ~15 per residue (of which ~9 per residue, corresponding to ~60% of the total number, are between unique proton pairs), subsequent increases in the number of restraints leads to less dramatic improvements (Fig. 3). This is due to the fact that a significant degree of information redundancy sets in above this limit.

(2) As a corollary to (1), the interproton distance vectors corresponding to the restraints in an ensemble of structures generated from a large number of loose approximate interproton distance restraints (i.e. an average of >15 per residue) are very well defined with ~80% of the vectors between unique proton pairs having a standard deviation of ≤0·1 Å (Table 1 and Fig. 1).

(3) The use of precise interproton distance restraints (represented by a restrictive square-well potential; eqn (3)), as opposed to loose approximate ones (cf. eqn (1)) has almost no effect on the attainable precision or accuracy (cf. Table 3; Figs 2 and 3).

(4) The precision of an NMR structure determination can be improved by either the use of accurate (as opposed to simply precise) interproton distance restraints (represented by a harmonic potential; eqn (2)) or by direct refinement against the NOE intensities (cf. eqn (6)). Interestingly, however, the structures obtained with the complete set of 854 accurate interproton distance restraints or with direct refinement against the corresponding 854 NOE intensities are no more accurate than those of the reference ensemble obtained with the 854 approximate interproton distance restraints (cf. Tables 3 and 5). Moreover, for a given level of ensemble precision, the accuracy of the mean co-ordinates for an ensemble of structures calculated with accurate interproton distance restraints is actually less than that of the mean co-ordinates for an ensemble of structures calculated with either approximate or precise interproton distance restraints (Fig. 4). Indeed, there is no difference in the accuracy of the mean co-ordinates for the ensemble of structures calculated with the complete set of 854 approximate or accurate interproton distance restraints (Table 3D), despite the fact that the precision of the former is less than that of the latter (Table 3A).

(5) The description of the non-bonded interactions, as evidenced, for example, by small variations in the effective hard sphere van der Waals radii used in the van der Waals repulsion term (cf. eqn (4)), has a significant effect on both precision and accuracy (Fig. 7). This imposes very real limits on the accuracy of an NMR protein structure determination and presents a major source of uncertainty, irrespective of the manner in which the geometric information of the NOE is incorporated into the target function. Indeed, even an alteration in the balance of forces within the target function, and in particular between the van der Waals term and the experimental NMR terms, is sufficient to have a significant effect on accuracy. This is

evidenced by the results obtained with accurate interproton distance restraints and full relaxation matrix refinement. In both these cases the "true" structure actually lies outside the ensemble of calculated structures, despite the fact that the latter are highly precise (cf. Tables 3 and 5).

What do these results imply in practice, particularly with regard to assessing the accuracy of a protein structure determination? It has been suggested (Thomas *et al.*, 1991; Nilges *et al.*, 1991) that the computation of an NMR *R*-factor between calculated and observed NOE intensities (cf. eqn (7)) would provide a more reliable method of assessment than the r.m.s. difference and violation count between calculated interproton distances and their corresponding target upper bounds for a set of approximate interproton distance restraints (in which the lower bound is set to 1·8 Å). The results presented suggest that this is not the case. Several criteria have to be met in an NMR structure determination, namely, the calculated structures must satisfy the experimental restraints as well as the restraints imposed by covalent geometry and stereochemistry (i.e. non-bonded contacts). However, these are not sufficient in themselves for assessing the quality of the NMR structure determination. For example, it is quite clear that if the average number of NOE restraints per residue is small, the structures generated will be of low accuracy despite the fact that they may exhibit very good agreement with the NOE restraints, be it in terms of violations or NOE intensities, as well as with the other restraints in the target function. Moreover, it is also clear that owing to the limited redundancy of the data, the structures will be unable to satisfy many of the remaining unassigned NOEs in the spectrum. Hence, one can only begin to talk seriously about an accurate structure determination when at least $\geq 90\%$ of the structurally useful NOEs have been assigned; that is to say when a significant degree of redundancy has set in. (This can be evaluated by carrying out a series of refinements using different subsets of interproton distance restraints or NOE intensities comprising, say, 90 to 95% of the total number, and calculating the agreement with the remaining 5 to 10% which are not included in the target function, a procedure similar in spirit to that of the free *R*-factor in X-ray crystallography (Brünger, 1992*b*).) Further, it is only under these circumstances that potential errors in NOE assignments can be assessed and corrected. The results summarized in Tables 4 and 5 indicate that at this stage of a protein NMR structure determination, any potential improvement that may be obtained by switching from a target function based on approximate interproton distance restraints to one based on direct refinement against NOE intensities, is likely to be insignificant. Moreover, given possibly large systematic errors in NOE intensities (up to 50 to 100%, see below), it seems likely in practice that any increased precision obtained by relaxation matrix refinement may be achieved at the expense of accuracy.

While relaxation matrix refinement can clearly account for multiple spin-relaxation pathways, inherent problems remain in terms of its practical applications, particularly with respect to the goal of obtaining accurate structures. For example, in a recent analysis of a 100 ps dynamics simulation of lysozyme, it has been shown that the rigid but correct structure would yield an R_1-factor of 22% for non-methyl internal proton pairs and 30% for pairs involving methyl protons, purely due to picosecond motions ≤ 10 ps (Post, 1992). Even larger discrepancies can be expected from internal motions which lie outside the extreme narrowing limit (i.e. motions with an internal correlation time τ_s in the range $0{\cdot}5\text{ ns} < \tau_s < \tau_R$, where τ_R is the rotational correlation time of the protein). Examples of such transitions have been seen as rare events in a recent 500 ps molecular dynamics simulation of interleukin-1β in water (Chandrasekhar *et al.*, 1992), and direct experimental evidence for such motions has been obtained from ^{15}N relaxation measurements (Clore *et al.*, 1990*a*,*b*; Stone *et al.*, 1992; Kördel *et al.*, 1992; Barbato *et al.*, 1992; Nicholson *et al.*, 1992; Powers *et al.*, 1992). These studies have also revealed the existence of heterogeneity arising from chemical exchange which will give rise to systematic errors in NOE intensities. While these two effects may generally be expected to involve exposed regions of the protein (e.g. loops and surface residues), this need not always be the case. Indeed, the recent joint NMR/X-ray refinement of the structure of interleukin-1β reveals that the side-chains of two completely buried leucine residues exist in two distinct χ_2 rotamer conformations (Shaanan *et al.*, 1992). Another source of error arises from practical considerations involved in the actual implementation of the NOE experiment. For example, it may not be feasible to allow sufficient time for complete relaxation back to equilibrium to occur between successive scans. This is particularly a problem in 3D and 4D NMR where the relaxation delay between scans has to be limited to a maximum of ~ 1 s in order to ensure that the experiment can be completed in a reasonable time frame. In addition, differential efficiency of transfer of magnetization from NH to ^{15}N and/or CH to ^{13}C *via* one-bond heteronuclear couplings in 3D and 4D experiments, arising from variations in linewidths, will introduce significant errors in NOE intensities. In contrast to relaxation matrix refinement, the use of loose approximate interproton distance restraints (e.g. 1·8 to 2·7 Å, 1·8 to 3·3 Å and 1·8 to 5 Å for strong, medium and weak NOE intensities, respectively, with additional corrections to the upper bounds in the case of methyl groups and non-stereospecifically assigned protons) avoids these problems (Wüthrich, 1986; Clore & Gronenborn, 1989*a*). The distance ranges are sufficiently generous to take into account the effects of spin diffusion. At the same time, internal motions (whose effect is simply to reduce the observed NOE intensity of a given proton–proton interaction) will not introduce errors, but rather simply increase the estimated range for a

particular interproton distance. The use of distinct cut-offs, on the other hand, can result in systematic errors for interproton distances whose values lie at the boundary of two distance ranges. This, however, can be corrected by examining the distribution of violations in the ensemble of calculated structures. If a particular interproton distance restraint is violated in nearly all the structures, even by as little as 0·1 Å, it is likely that it should either be reclassified into the next class (i.e. strong to medium, medium to weak) or that errors in NOE assignments are present.

The results presented in this paper also permit one to obtain an approximate estimate of accuracy from the precision of the ensemble of calculated structures. For a given non-bonded potential in the target function, the ratio of ensemble precision to ensemble accuracy is approximately independent of the number, precision or accuracy of the interproton distance restraints with an average value of 0·65, 0·75 and 0·7 for the backbone atoms, all atoms and all ordered atoms, respectively (Table 3). Independently, uncertainties in the values of the hard sphere van der Waals radii will also reduce the ratio of precision to accuracy (cf. Fig. 7). Examination of the van der Waals parameters for a variety of empirical force fields suggests that the values of the effective hard sphere van der Waals radii given by $r_{vdw}(\text{eff}) = s_{vdw} \cdot r_{vdw}$ can vary within the range of $s_{vdw} = 0{\cdot}75$ to 0·85 using the van der Waals radii of the CHARMM PARAM19/PARAM20 force field for r_{vdw}. This, for example, encompasses the hard sphere van der Waals radii used in the programs DISMAN (Braun & Go, 1985) and DIANA (Güntert *et al.*, 1991; cf. Table 2). The results with $s_{vdw} = 0{\cdot}85$ have the lowest ratio of precision to accuracy (~0·6, ~0·8 and ~0·7 for backbone atoms, all atoms and all ordered atoms) and therefore probably represent an upper limit of the effect of uncertainties in the van der Waals radii on these values. Hence, the overall ratio of ensemble precision to ensemble accuracy is the product of these two factors which yields average values of ~0·4, ~0·6 and ~0·5 for backbone atoms, all atoms and all ordered atoms. If we consider that the precision of an ensemble of structures attainable in the relaxation matrix refinement calculations with the 854 NOE restraints represents the best that can be achieved in practice, then the likely best upper limits of ensemble accuracy that can be achieved in an NMR structure determination are ~0·4 Å for backbone atoms, ~0·8 Å for all atoms and ~0·5 Å for all ordered atoms. These values are comparable to those of a 2 Å resolution crystal structure, as judged by the r.m.s. differences between independently solved crystal structures of the same protein in the same crystal form (Clore & Gronenborn, 1991c). However, these estimates do not take into account the potential systematic errors in relaxation matrix refinement arising from internal motions. Hence, if one considers that the precision of the ensemble of structures calculated with the 854 approximate interproton restraints represents a more realistic estimate for an upper limit on ensemble precision, then the corresponding limits on ensemble accuracy would be ~0·6 Å for backbone atoms, ~1·1 Å for all atoms and ~0·8 Å for all ordered atoms. The accuracy of the mean co-ordinates of a given ensemble is significantly higher than the average accuracy of the individual structures within an ensemble. From the plots shown in Figure 4, the accuracy of the mean co-ordinates reaches a limiting value of ~0·1 Å. Adding in an uncertainty of 0·2 to 0·3 Å (cf. Fig. 7) attributable to the non-bonded contacts suggests that the actual limiting accuracy of the mean co-ordinates is 0·3 to 0·4 Å. Given that there are a finite number of short interproton distance contacts that can be observed experimentally, this translates to a likely upper limit on the attainable accuracy of the mean co-ordinates of 0·4 to 0·5 Å for backbone atoms, 0·6 to 0·7 Å for all atoms and 0·5 to 0·6 Å for all ordered atoms. In this light, it is perhaps not surprising that even for the most precise NMR structures determined to date, the backbone atomic r.m.s. differences between them and the corresponding X-ray structure(s) range from 0·7 to 1·2 Å (Billeter *et al.*, 1989, 1992; Clore & Gronenborn, 1991*c*,*d*; Moore *et al.*, 1991).

This work was supported by the AIDS Targeted Antiviral Program of the Office of the Director of the National Institutes of Health (G.M.C. and A.M.G.). M.A.R. was supported by the Howard Hughes Medical Institute–National Institutes of Health Research Scholars Program. We thank Dr Attila Szabo for stimulating discussions.

References

Barbato, G., Ikura, M., Kay, L. E., Pastor, R. W. & Bax, A. (1992). Backbone dynamics of calmodulin studied by ^{15}N relaxation using inverse detected two-dimensional NMR spectroscopy: the central helix is flexible. *Biochemistry*, **31**, 5269–5278.

Billeter, M., Kline, A. D., Braun, W., Huber, R. & Wüthrich, K. (1989). Comparison of the high-resolution structures of the α-amylase inhibitor tendamistat determined by nuclear magnetic resonance in solution and by X-ray crystallography in single crystals. *J. Mol. Biol.* **206**, 677–687.

Billeter, M., Vendrell, J., Wider, G., Aviles, F. X., Coll, M., Gausch, A., Huber, R. & Wüthrich, K. (1992). Comparison of the NMR solution structure with the X-ray crystal structure of the activation domain from procarboxypeptidase B. *J. Biomolec. NMR*, **2**, 1–10.

Boelens, R., Koning, T. M. G. & Kaptein, R. (1988). Determination of biomolecular structures from proton–proton NOEs using a relaxation matrix approach. *J. Mol. Struct.* **173**, 299–311.

Boelens, R., Koning, T. M. G., Van der Marel, G. A., van Boom, J. H. & Kaptein, R. (1989). Iterative procedure for structure determination from proton–proton NOEs using a full relaxation matrix approach. Application to a DNA octamer. *J. Magn. Reson.* **82**, 290–308.

Borgias, B. A. & James, T. L. (1988). COMATOSE, a method for constrained refinement of macro-

molecular structure based on two-dimensional nuclear Overhauser spectra. *J. Magn. Reson.* **79**, 493–512.

Borgias, B. A. & James, T. L. (1990). MARDIGRAS: a procedure for matrix analysis of relaxation for discerning geometry of aqueous structures. *J. Magn. Reson.* **87**, 475–487.

Borgias, B. A., Gochin, M., Kerwood, D. J. & James, T. L. (1990). Relaxation matrix analysis of 2D NMR data. *Progr. NMR Spectrosc.* **22**, 83–100.

Braun, W. & Go, N. (1985). Calculation of protein conformation by proton–proton distance constraints: a new efficient algorithm. *J. Mol. Biol.* **186**, 611–626.

Brooks, B. R., Bruccoleri, R. E., Olafson, B. D., States, D. J., Swaminathan, S. & Karplus, M. (1983). CHARMM: a program for macromolecular energy minimization, and dynamics calculations. *J. Comput. Chem.* **4**, 187–217.

Brünger, A. T. (1992*a*). XPLOR Version 3.0 User Manual, Yale University.

Brünger, A. T. (1992*b*). Free *R*-value: a novel statistical quantity for assessing the accuracy of crystal structures. *Nature (London)*, **355**, 472–474.

Brünger, A. T., Clore, G. M., Gronenborn, A. M. & Karplus, M. (1986). Three-dimensional structures of proteins determined by molecular dynamics with interproton distance restraints: application to crambin. *Proc. Nat. Acad. Sci., U.S.A.* **83**, 3801–3805.

Brünger, A. T., Clore, G. M., Gronenborn, A. M. & Karplus, M. (1987). Solution conformations of human growth hormone releasing factor: comparison of the restrained molecular dynamics and distance geometry methods for a system without long range distance data. *Protein Eng.* **5**, 399–406.

Chandrasekhar, I., Clore, G. M., Szabo, A., Gronenborn, A. M. & Brooks, B. R. (1992). A 500 ps molecular dynamics simulation study of interleukin-1β in water: correlation with nuclear magnetic resonance spectroscopy and crystallography. *J. Mol. Biol.* **226**, 239–250.

Clore, G. M. & Gronenborn, A. M. (1989*a*). Determination of three-dimensional structures of proteins and nucleic acids in solution by nuclear magnetic resonance spectroscopy. *CRC Crit. Rev. Biochem. Mol. Biol.* **24**, 479–564.

Clore, G. M. & Gronenborn, A. M. (1989*b*). How accurately can interproton distances in macromolecules really be determined by full relaxation matrix analysis of nuclear Overhauser enhancement data? *J. Magn. Reson.* **84**, 398–409.

Clore, G. M. & Gronenborn, A. M. (1991*a*). Structures of larger proteins in solution: three- and four-dimensional heteronuclear NMR spectroscopy. *Science*, **252**, 1390–1399.

Clore, G. M. & Gronenborn, A. M. (1991*b*). Two, three and four-dimensional NMR methods for obtaining larger and more precise three-dimensional structures of proteins in solution. *Annu. Rev. Biophys. Biophys. Chem.* **20**, 29–63.

Clore, G. M. & Gronenborn, A. M. (1991*c*). Comparison of the solution nuclear magnetic resonance and X-ray crystal structures of human recombinant interleukin-1β. *J. Mol. Biol.* **221**, 47–53.

Clore, G. M. & Gronenborn, A. M. (1991*d*). Comparison of the solution nuclear magnetic resonance and crystal structures of interleukin-8: possible implications for the mechanism of receptor binding. *J. Mol. Biol.* **217**, 611–620.

Clore, G. M. & Gronenborn, A. M. (1991*e*). Comparison of NMR and X-ray structures of hirudin. In *Computational Aspects of the Study of Biological Macromolecules by Nuclear Magnetic Resonance Spectroscopy* (Hoch, J. C., Poulsen, F. M. & Redfield, C., eds), pp. 57–66, NATO ASI Series, Plenum Press, New York.

Clore, G. M., Gronenborn, A. M., Brünger, A. T. & Karplus, M. (1985). The solution conformation of a heptadecapeptide comprising the DNA binding helix F of the cyclic AMP receptor protein of *Escherichia coli*: combined use of ^{1}H-nuclear magnetic resonance and restrained molecular dynamics. *J. Mol. Biol.* **186**, 435–455.

Clore, G. M., Nilges, M., Sukumaran, D. K., Brünger, A. T., Karplus, M. & Gronenborn, A. M. (1986*a*). The three-dimensional structure of α1-purothionin in solution: combined use of nuclear magnetic resonance, distance geometry and restrained molecular dynamics. *EMBO J.* **5**, 2729–2735.

Clore, G. M., Brünger, A. T., Karplus, M. & Gronenborn, A. M. (1986*b*). Application of molecular dynamics with interproton distance restraints to three-dimensional protein structure determination: a model study of crambin. *J. Mol. Biol.* **191**, 523–551.

Clore, G. M., Gronenborn, A. M., Nilges, M. & Ryan, C. A. (1987*a*). The three-dimensional structure of potato carboxypeptidase inhibitor in solution: a study using nuclear magnetic resonance, distance geometry and restrained molecular dynamics. *Biochemistry*, **26**, 8012–8023.

Clore, G. M., Gronenborn, A. M., James, M. N. G., Kjaer, M., McPhalen, C. A. & Poulsen, F. M. (1987*b*). Comparison of the solution and X-ray structures of barley serine proteinase inhibitor 2. *Protein Eng.* **1**, 313–318.

Clore, G. M., Szabo, A., Bax, A., Kay, L. E., Driscoll, P. C. & Gronenborn, A. M. (1990*a*). Deviations from the simple two parameter model free approach to the interpretation of ^{15}N nuclear magnetic relaxation of proteins. *J. Amer. Chem. Soc.* **112**, 4989–4991.

Clore, G. M., Driscoll, P. C., Wingfield, P. T. & Gronenborn, A. M. (1990*b*). Analysis of backbone dynamics of interleukin-1β using two-dimensional inverse detected heteronuclear ^{15}N–^{1}N NMR spectroscopy. *Biochemistry*, **29**, 7387–7401.

Clore, G. M., Wingfield, P. T. & Gronenborn, A. M. (1991). High resolution three-dimensional structure of interleukin-1β in solution by three- and four-dimensional nuclear magnetic resonance spectroscopy. *Biochemistry*, **30**, 2315–2323.

Dauber-Osguthorpe, P., Roberts, V. A., Osguthorpe, D. J., Woldd, J., Genest, M. & Hagler, A. T. (1988). Structure and energetics of ligand binding to proteins: *Escherichia coli* dihydrofolate reductase-trimethoprim, a drug-receptor system. *Proteins: Struct. Funct. Genet.* **4**, 31–47.

Gronenborn, A. M., Filpula, D. R., Essig, N. Z., Achari, A., Whitlow, M., Wingfield, P. T. & Clore, G. M. (1991). A novel highly stable fold of the immunoglobulin binding domain of streptococcal protein G. *Science*, **253**, 657–661.

Güntert, P., Braun, W. & Wüthrich, K. (1991). Efficient computation of three-dimensional protein structures in solution from nuclear magnetic resonance data using the program DIANA and the supporting programs CALIBA, HABAS and GLOMSA. *J. Mol. Biol.* **217**, 517–530.

Kördel, J., Skelton, N. J., Akke, M., Palmer, A. G., III &

Chazin, W. J. (1992). Backbone dynamics of calcium-loaded calbindin D9k studied by two-dimensional proton-detected ^{15}N NMR spectroscopy. *Biochemistry*, **31**, 4856–4866.

Kuszewski, J., Nilges, M. & Brünger, A. T. (1992). Sampling and efficiency of metric matrix distance geometry: a novel partial metrization algorithm. *J. Biomolec. NMR*, **2**, 33–56.

Momany, F. A., Carruthers, L. M., McGuire, R. F. & Scheraga, H. A. (1974). Intermolecular potentials from crystal data III. Determination of empirical potentials and application to the packing configurations and lattice energies in crystals of hydrocarbons, carboxylic acids, amides and amides. *J. Phys. Chem.* **78**, 1595–1620.

Moore, J. M., Lepre, C., Gippert, G. P., Chazin, W. J., Case, D. A. & Wright, P. E. (1991). High resolution solution structure of reduced French bean plastocyanin and comparison with the crystal structure of poplar plastocyanin. *J. Mol. Biol.* **221**, 533–555.

Nicholson, L. K., Kay, L. E., Baldisseri, D. M., Arango, J., Young, P. E., Bax, A. & Tochia, D. A. (1992). Dynamics of methyl groups in proteins as studied by proton detected ^{13}C NMR spectroscopy. Application to the leucine residues of Staphylococcal nuclease. *Biochemistry*, **31**, 5253–5263.

Nilges, M., Clore, G. M. & Gronenborn, A. M. (1988). Determination of three-dimensional structures of proteins from interproton distance data by hybrid distance geometry-dynamical simulated annealing calculations. *FEBS Letters*, **239**, 317–324.

Nilges, M., Clore, G. M. & Gronenborn, A. M. (1990). ^{1}H-NMR stereospecific assignments by conformational database searches. *Biopolymers*, **29**, 831–822.

Nilges, M., Habazettl, J., Brünger, A. T. & Holak, T. A. (1991). Relaxation matrix refinement of the solution structure of squash trypsin inhibitor. *J. Mol. Biol.* **219**, 499–510.

Nilsson, L. & Karplus, M. (1986). Empirical energy functions for energy minimization and dynamics of nucleic acids. *J. Comput. Chem.* **7**, 691–716.

Post, C. B. (1992). Internal motional averaging and three-dimensional structure determination by nuclear magnetic resonance. *J. Mol. Biol.* **224**, 1087–1101.

Post, C. B., Meadows, R. P. & Gorenstein, D. G. (1990). On the evaluation of interproton distances for three-dimensional structure determination by NMR using a relaxation rate matrix analysis. *J. Amer. Chem. Soc.* **112**, 6796–6803.

Powers, R., Clore, G. M., Stahl, S. J., Wingfield, P. T. & Gronenborn, A. M. (1992). Analysis of the backbone dynamics of the ribonuclease H domain of the immunodeficiency virus reverse transcriptase using ^{15}N relaxation measurements. *Biochemistry*, **31**, 9150–9157.

Reiher, W. E. (1985). Theoretical studies of hydrogen bonding. Ph.D. thesis, Harvard University, Cambridge, MA.

Shaanan, B., Gronenborn, A. M., Cohen, G. H., Gilliland, G. L., Veerapandian, B., Davies, D. R. & Clore, G. M. (1992). Combining experimental information from crystal and solution studies: joint X-ray and NMR refinement. *Science*, **257**, 961–964.

Stone, M. J., Fairbrother, W. J., Palmer, A. G., III, Reizer, J., Saier, M. H. & Wright, P. E. (1992). Backbone dynamics of the *Bacillus subtilis* glucose permease IIA domain determined from ^{15}N relaxation measurements. *Biochemistry*, **31**, 4394–4406.

Thomas, P. D., Basus, V. J. & James, T. L. (1991). Protein solution structure determination using distances from two-dimensional nuclear Overhauser effect experiments. Effects of approximations on the accuracy of derived structures. *Proc. Nat. Acad. Sci., U.S.A.* **88**, 1237–1241.

Weiner, S. J., Kollman, P. A., Case, D. A., Singh, U. C., Ghio, C., Alagona, G., Profeta, S. & Weiner, P. (1984). A new force field for molecular mechanical simulation of nucleic acids and proteins. *J. Amer. Chem. Soc.* **106**, 765–784.

Weiner, S. J., Kollman, P. A., Nguyen, D. T. & Case, D. A. (1986). An all-atom force field for simulations of proteins and nucleic acids. *J. Comput. Chem.* **7**, 230–252.

Wüthrich, K. (1986). *NMR of Proteins and Nucleic Acids*. Wiley, New York.

Yip, P. & Case, D. A. (1991). A new method for refinement of macromolecular structures based on nuclear Overhauser effect spectra. *J. Magn. Reson.* **83**, 643–648.

Edited by W. Hendrickson